VPI - ENGR.98.166
Proposal # 98-0447-10
NAG-1-2001

Final Report

Active Control of Inlet Noise on the JT15D Turbofan Engine

prepared by:

Jerome P. Smith
Florence V. Hutcheson
Ricardo A. Burdisso
Chris R. Fuller
Vibration and Acoustics Laboratories
Department of Mechanical Engineering
Virginia Polytechnic Institute & State University
Blacksburg, VA 24061-0238

for

NASA Langley Research Center
Aeroacoustics Branch
Hampton, VA

Department of Mechanical Engineering
Virginia Polytechnic Institute & State University
Blacksburg, VA 24061-0238
January, 1999

ABSTRACT

This report presents the key results obtained by the Vibration and Acoustics Laboratories at Virginia Tech over the year from November 1997 to December 1998 on the Active Noise Control of Turbofan Engines research project funded by NASA Langley Research Center. The concept of implementing active noise control techniques with fuselage-mounted error sensors is investigated both analytically and experimentally. The analytical part of the project involves the continued development of an advanced modeling technique to provide prediction and design guidelines for application of active noise control techniques to large, realistic high bypass engines of the type on which active control methods are expected to be applied. Results from the advanced analytical model are presented that show the effectiveness of the control strategies, and the analytical results presented for fuselage error sensors show good agreement with the experimentally observed results and provide additional insight into the control phenomena. Additional analytical results are presented for active noise control used in conjunction with a wavenumber sensing technique. The experimental work is carried out on a running JT15D turbofan jet engine in a test stand at Virginia Tech. The control strategy used in these tests was the feedforward Filtered-X LMS algorithm. The control inputs were supplied by single and multiple circumferential arrays of acoustic sources equipped with neodymium iron cobalt magnets mounted upstream of the fan. The reference signal was obtained from an inlet mounted eddy current probe. The error signals were obtained from a number of pressure transducers flush-mounted in a simulated fuselage section mounted in the engine test cell. The active control methods are investigated when implemented with the control sources embedded within the acoustically absorptive material on a passively-lined inlet. The experimental results show that the combination of active control techniques with fuselage-mounted error sensors and passive control techniques is an effective means of reducing radiated noise from turbofan engines. Strategic selection of the location of the error transducers is shown to be effective for reducing the radiation towards particular directions in the farfield. An analytical model is used to predict the behavior of the control system and to guide the experimental design configurations, and the analytical results presented show good agreement with the experimentally observed results.

1. INTRODUCTION

This report presents the key results of the research performed by the Virginia Tech Vibration and Acoustic Laboratories over the year from November 1997 to December 1998 on the JT15D turbofan engine project funded by NASA Langley Research Center. The purpose of this research is to investigate the potential of using active control methods in conjunction with fuselage-mounted error sensors for reducing the noise radiated from a turbofan engine. The general concept is depicted in Figure 1.1, which shows a Boeing 717 airplane equipped with active and passive control components on the inlet of the turbofan engine, and far-field fuselage-mounted error transducers flush-mounted into the side of the airplane fuselage. Circumferential arrays of acoustic sources, flush mounted in the inlet wall are used to inject sound upstream of the fan and generate the acoustic field necessary to cancel the tone noise radiated at the fan blade passing frequency (BPF) and the associated harmonics. These active components are embedded within the inlet passive liner material, which achieves some reduction of the broadband noise, and reduces some of the tonal noise radiated to the sidelines of the engine. The error information which guides the convergence of the control system is obtained from the microphones mounted on the fuselage. Virginia Tech has an operating JT15D turbofan engine in a test cell at the Virginia Tech Airport, as well as the facilities to develop control system components and analytical models investigating the potential of this technique. These facilities provide a unique environment for the design and direct implementation and evaluation of these methods in a very realistic setting. This is an ongoing research project which has the following overall objectives:

1) To develop advanced modeling techniques for the design and optimization of an active control system with application to larger high bypass engines. (F. Hutcheson, R. Burdisso, and C. Fuller)

2) To experimentally demonstrate useful active control of turbofan inlet noise using realistic sensors and actuators, and passive components on a running JT15D turbofan engine. (J. Smith and R. Burdisso)

This report is organized with one section devoted to each of the two above aspects. Section 2 presents the advanced analytical model with results of applying active control to a larger high-bypass engine, using both fuselage-mounted error sensing techniques and inlet wavenumber error sensors. Section 3 contains the experimental setup and the results obtained for applying passive-active control to the JT15D turbofan engine. Section 4 contains a summary of the main conclusions and accomplishments.

2. ADVANCED MODELING OF ACTIVE CONTROL OF FAN NOISE FOR ULTRA HIGH BYPASS TURBOFAN ENGINES

The models that are currently available to conduct active noise control studies of fan noise for turbofan engines have some or all of the following limitations: they do not

account for the reflection from the duct openings nor for the presence of evanescent modes in the duct; they do not include radiation from the outlet and do not have lining capabilities. Therefore, the first objective of this study was to develop a more advanced model of active noise control for turbofan engines, i.e., a model that does not have the limitations mentioned previously. The second objective of this work was to use that model to investigate the performance of active noise control in reducing fan noise for ultra high bypass turbofan engines. Pure active control techniques as well as hybrid control techniques were studied.

2.1 Active noise control model

This model was developed by implementing active noise control to the duct fan noise prediction code TBIEM3D that was developed by Dr. Dunn, Dr. Farassat and Dr. Tweed at NASA Langley Research Center. This model is based on a boundary integral equation method and assumes that all acoustic processes are linear, generate spinning modes and occur in a uniform flow field. A schematic of the model is shown in Figure 2.1. We considered a duct of cylindrical profile and finite length with a rigid exterior wall and a rigid or lined inner wall. The fan noise that was initially generated by a circumferential array of spinning point dipoles is now modeled by a circumferential array of spinning line sources with linearly distributed strength. This ducted fan was assumed to be placed in a uniform flow. Reflection from the duct openings was taken into account as well as the presence of the modes that are cut off and are decaying in the duct. Forward, as well as backward, external acoustic radiation were computed. The control sources that generate the secondary field were modeled by point monopoles placed along the duct inner wall.

2.2 Active noise control study for a ultra high bypass turbofan engine

This model was used to investigate the potential that active noise control techniques have for reducing fan noise on a large turbofan engine. Thus, a case with a duct of radius 1.5 m and an inlet and outlet length each of 1.74 m was studied. These dimensions are representative of those associated with an ultra high bypass turbofan engine prototype being developed by Pratt and Whitney. A BPF of 1000 Hz, and a uniform flow Mach number of 0.25, which is representative of landing or take off conditions, were considered. Since future engine designs might leave the fourth or fifth order circumferential modes cut on, the generation of the fourth order circumferential modes was also considered.

A plot of the resulting pressure field in a plane containing the axis of the duct is presented in Figure 2.2. This plot is composed of 200 by 200 computation points and was calculated in approximately 10 minutes on a PC. Six fourth order circumferential modes were cut on and propagated through the inlet and outlet of the duct. The cut-off ratios of the first and last modes that were cut on (i.e., the (4,0) and (4,5) modes) are 5.34 and 1.26 respectively. The goal was then to reduce the noise that radiates within the 40° to 155°

sector (sector counted from the inlet opening and with respect to the axis of the duct), which is believed to strongly affect the EPNL.

2.2.1 Pure passive control

The amount of reduction in sound power level that could be achieved within the target sector (the 40° to 155° sector) using pure passive control was first determined. It was assumed that the duct would be lined over its entire length, except at the tip of the duct inlet and outlet. The attenuation in sound power level that could be obtained in other sectors of the far field using various values of the liner impedance was also computed. Only impedance values representative of realistic liners were considered.

The reduction in sound power level that could be achieved within different sectors of the far field is shown in Figure 2.3. From this figure it is observed that, as expected, the liners worked poorly in attenuating the noise radiated towards the region close to the duct axis and worked best in reducing the noise radiated toward the sideline of the duct. Up to 1.5 dB reduction in sound power level could be achieved within the 0° to 40° sector, 4.6 dB for the 40° to 70° sector, and 14.4 dB for the 70° to 125° sector. Thus, within the target sector, the passive control system was able to achieve a maximum reduction in sound power level of 4.6 dB.

Next, it was determined whether the levels of reduction that were achieved in the target sector with the pure passive control system could be improved when using active control techniques.

2.2.2 Fuselage error sensors technique

A schematic of the control system is presented in Figure 2.4. An axial array of error sensors was placed along the aircraft fuselage, 6 m from the axis of the duct. This distance was estimated from studying schematics of large commercial planes with wing mounted engines. The error sensors were placed within the 40° to 70° sector when controlling the inlet fan noise radiation, or within the 125° to 155° sector when controlling the outlet radiation. One or two circumferential arrays of control sources were placed in the duct and used to generate the control field.

a) Pure ANC

The duct inner wall was first considered to be rigid. Using an array of three fuselage error sensors placed within the 40° to 70° sector and a single array of control sources, the axial location of the control source array that would lead to a maximum reduction in the target sector was determined by changing the axial position of the control source array, which was stepped along the duct length from 1.7 m downstream of the fan to 1.7 m upstream of the fan in 0.1 m increments. The results obtained are presented in Figures 2.5(a) and 2.5(b). The maximum reduction in sound power level that could be achieved in the target sector was 2.5 dB, and was achieved when the control source array was placed

0.2 m upstream of the fan. From the table of Figure 2.5(b) it can be seen that the maximum level of reduction achieved in the target sector (2.5 dB) was not obtained for the control system configuration that led to a maximum level of reduction in the 40° to 70° sector (where the error sensors were located). Instead, it was achieved for a configuration of the control system that avoided the creation of spillover in the region of the far field of the outlet, while still maintaining a good level of attenuation within the 40° to 70° sector.

The reduction in sound power level that could be achieved in the target sector for different axial locations of a single control source array was recomputed by placing an array of seven error sensors, instead of three along the fuselage within the 40° to 70° sector . The results are presented in Figures 2.6(a) and 2.6(b). It is observed that a reduction in sound power level of 2.9 dB could be obtained in the target sector when the control source array was located 0.2 m upstream of the fan. This is an improvement of 0.4 dB over the preceding case where an array of only 3 error sensors was used. Thus, the use of additional error sensors did not lead to a very significant improvement in the maximum level of reduction that could be achieved in the target sector. The maximum level of reduction for the target sector was obtained, as in the preceding case, for a configuration of the control system that led to a simultaneous reduction of the noise that radiates in the far field of the inlet and outlet. This optimum solution is seen to remain sensitive to the axial location of the control source array.

A comparison of the reduction levels obtained within the 40° to 70° sector for different locations of the control source array, where using seven versus three error sensors, is presented in Figure 2.7. It can be seen that improved coverage by the error sensors of the 40° to 70° sector increased the number of control source array locations that led to a reduction in sound power level and almost eliminated the occurrence of spillover in this 40° to 70° sector. This resulted both in an overall decrease in the levels of spillover that could occur within the target sector, and also in an increase in the number of configurations of the control system that assured a reduction in sound power level in the target sector.

Next, the results discussed above were compared with the ones obtained while using two control source arrays, instead of one, to generate the control field.

First, an array of three fuselage error sensors was placed within the 40° to 70° sector. The axial positions of the two control source arrays were stepped along the duct inlet and outlet in 10 cm increments in order to find the configuration of the control system that would lead to a maximum reduction in sound power level in the target sector. The results are presented in Figures 2.8(a) and 2.8(b).

The maximum attenuation that could be obtained was 5.3 dB when the control source arrays were located, respectively, 0.1 m and 0.4 m upstream of the fan. This is an improvement of 1.8 dB over the single control source array case. This optimum configuration of the control system led simultaneously to a reduction of 5.2 dB within the 40° to 70° sector, and to a reduction of 4.8 dB within the 125° to 155° sector. It can be

seen that, the addition of a second control source array improved the ability of the control system to simultaneously control the modes that propagated through the inlet and outlet of the duct. It was also noted that this active noise control system configuration could lead to a reduction of up to 7.3 dB in sound power level for the 40° to 70° sector, which is an increase of 3.55 dB over the level of reduction that could be achieved with a single control source array. Thus, the addition of a second control source array to the control system increased the system's controllability over the higher order radial modes that radiated within the target sector, or more precisely, within the 40° to 70° sector. Although the controllability of the system over the propagating modes was improved, the optimum solution remained very sensitive to the location of the control source arrays. A reduction of 4.3 dB could be obtained with less sensitivity.

Placing seven error sensors instead of three along the fuselage, within the 40° to 70°, sector did not significantly improve the maximum reduction in sound power level that could be achieved in the target sector. Figures 2.9(a), 2.9(b), 2.9(c) and 2.9(d) show the sound power level reduction achieved for the 40° to 70° sector and for the 125° to 155° sector using three or seven fuselage error sensors. It is observed that while reduction in sound power level could be achieved relatively easy within the sector containing the error sensors, spillover would dominate in the far field of the outlet. However, it is noted that, for both of these sectors, the placement of additional error sensors within the 40° to 70° sector increased the number of control source array locations that led to reductions in sound power level and reduced the levels of possible spillovers. These two effects are also observed for the 40° to 155° sector (cf. Figures 2.10(a) and 2.10(b)). Thus, a larger number of control source array locations that led to noise reductions in the target sector could be obtained with seven error sensors than with three, and a maximum spillover of only 2.6 dB could occur with seven error sensors versus a maximum of 10 dB with the three error sensors case.

Therefore, using the pure active noise control fuselage error sensors technique, it was observed that:

(i) Using two control source arrays versus one increased controllability over the propagating modes and could increase, by up to 3 dB, the reduction that could be achieved in the target sector.

(ii) Using seven versus three error sensors did not significantly change the levels of reduction that could be achieved in the target sector, but it significantly increased the number of control source array locations that led to reductions in the target sector and reduced the level of possible spillovers.

(iii) By using two control source arrays and seven sensors, the active noise control system could match or exceed the performance of the optimum pure passive control case.

b) Hybrid control:

Next, it was determined whether the above mentioned results could be improved by adding a liner to the active noise control system; that is by using a hybrid control system instead of a pure active or pure passive control system. Two different hybrid control systems were studied. For both of these systems, the duct was considered to be lined over its entire length except at the tip of the duct inlet and outlet.

In the first case, one control source array and an axial array of three fuselage error sensors placed along the fuselage, within the 40° to 70° sector, were considered for the active part of the control system. The maximum reduction in sound power level that could be achieved in the target sector by this hybrid control system was then determined by simultaneously optimizing the impedance of the liner and the axial location of the control source array. The optimum configuration of the control system led to a maximum reduction of 8.4 dB. It was achieved for a liner specific impedance of 1.7+2.8i, when the control source array was located 0.2 m upstream of the fan.

The robustness of this optimum solution with respect to the location of the control source array was next evaluated. To do so, the attenuation in sound power level that could be achieved in the target sector by the hybrid control system was computed for various locations of the control source array, while the duct wall was lined with the optimum liner of specific impedance 1.7+2.8i . These results are presented in Figure 2.11(a). This figure shows that although at least 4 dB of reduction could be achieved for almost all possible axial locations of the control source array, the optimum solution remains sensitive to variation in the control source array location.

The robustness of this optimum solution with respect to the location of the control source array was also studied. The reduction in sound power level that could be achieved in the target sector was computed for various values of the liner impedance, while the control source array was fixed at its optimum location (0.2 m upstream of the fan). The results are presented in Figure 2.11(b). From this figure it is seen that levels of reduction close to the maximum could be obtained for a large number of impedance values. Thus, the optimum solution is robust with respect to variation in liner impedance.

In the second case, two control source arrays and an axial array of seven fuselage error sensors placed within the 40° to 70° sector were considered for the active control part of the hybrid system. The dimensions of the liner remained unchanged. Again, the control source arrays locations and the liner impedance combination that would lead to the best reduction in the 40° to 155° sector were determined. The best attenuation that could be achieved was 10.2 dB with a liner specific impedance of 1.7+2.8i and with the control arrays placed 0.2 m and 1.6 m, respectively, upstream of the fan. Figures 2.12(a) and 2.12(b) show the robustness of the optimum solution with respect to the liner impedance and with respect to the control source arrays locations. Again, the optimum solution appears to be more sensitive to the location of the control source arrays than to the liner impedance. Nevertheless, reduction occurred for almost all control source array locations.

Thus, using this hybrid control technique, it was observed that:

(i) The hybrid system increased the reduction in sound power level by 6 dB in the target sector over the pure active or passive noise control systems.

(ii) The presence of the liner greatly increased the number of control source array locations for which reduction occurred in the target sector.

(iii) The optimum solution was very robust with respect to the liner impedance and less with respect to the control source array location.

c) Control of inlet and outlet radiation

Placing the fuselage error sensors in the far field of the inlet insured a good reduction in that region of the far field; however, it also led to considerable spillover in the far field of the outlet, hindering the level of noise reduction and the robustness of the optimum solution.

Therefore, in addition to placing an axial array of three error sensors along the fuselage within the 40° to 70° sector, an array of three error sensors was also placed along the fuselage within the 125° to 155° sector. Pure active as well as hybrid control systems were studied with this configuration of the error sensors using one or two arrays of control sources. The maximum attenuation in sound power level that could be achieved in the target sector with each of these control systems is presented in Figure 2.13(a). With the pure active control system, the possible reduction was up to 2.03 dB when one control source array was used, and up to 4.3 dB when two control source arrays were used. With the hybrid system, a reduction up to 7.3 dB could be achieved using one control source array and up to 9.6 dB with two control source arrays. These levels are slightly lower than the ones that could be achieved when three error sensors were placed only within the 40° to 70° sector (cf. Figure 2.13(b)).

Figures 2.14(a), 2.14(b) and 2.14(c) show, for the sectors spanning 40° to 155°, 40° to 70° and 125° to 155°, the reduction in sound power level that was achieved by the pure active control system for various locations of the two control source arrays used. It can be seen that the control source arrays locations that led to reduction in the target sector correspond well to the ones that also led to reduction in the 40° to 70° sector, but did not correspond well to the ones that led to reduction in the 125° to 155° sector. This was also observed for the other configurations of the control system being studied. This seemed to indicate that reducing the sound power level within the 40° to 70° sector would achieve better results for the overall reduction in the target sector than reducing the sound power level in the 125° to 155° sector. By adding error sensors to the far field of the outlet, less reduction was achieved in the 40° to 70° sector since the control system was made to perform at both the inlet and outlet regions of the far field. This impacted negatively the

maximum level of overall reduction for the target sector, although better reduction (or at least less spillover) was obtained in the 125° to 155° sector as a result of the outlet far field error sensors.

The addition of error sensors to the far field of the outlet did not increase the maximum level of reduction for the target sector, but it did improve the robustness of the optimum solution by increasing the number of control source array locations that led to a reduction in the target sector. Although this was verified for each of the systems being studied, only one will be discussed. For each of the two hybrid control systems under consideration, the impedance of the liner was fixed to its optimum value. That is, the value that led each of these systems to achieve their maximum level of reduction in the target sector. Figures 2.15(a) and 2.15(b) show the reduction in sound power level that could be achieved in the 125° to 155° and 40° to 155° sectors by using an hybrid control system with three error sensors placed in the far field of the inlet and outlet and two control source arrays. These results were compared with the ones that were achieved by the hybrid control system when three error sensors were placed in the far field of the inlet only (cf. Figures 2.15(c) and 2.15(d)). These reduction levels were computed as functions of the location of the control source arrays.

Therefore, by adding fuselage error sensors to the far field of the outlet, it was observed that:

(i) It increased the number of locations of the control source arrays that led to reduction in sound power level in the target sector.

(ii) It reduced the level of possible spillover.

(iii) It decreased the peak value of sound power level reduction (this might not be the case for an annular duct).

2.2.3 Wavenumber error sensors technique

With this technique, instead of minimizing the pressure at error sensors placed in the far field of the duct inlet or outlet, certain components of the wavenumber spectrum are minimized in an attempt to reduce the acoustic radiation towards specific directions in the far field. The basic idea is that by minimizing a specific wavenumber component of the spectrum, the mode that propagates in the duct with that specific axial wavenumber would be indirectly targeted, and therefore noise reduction would be achieved in the region of the far field where that mode would have been radiated. Thus, by targeting the lower wavenumber components one should expect to attenuate the radiation toward the sideline of the duct, while minimizing the higher wavenumbers should reduce the noise radiated toward the duct axis.

Figure 2.16 describes a schematic of the control system used. An axial array of pressure sensors was placed along the duct inlet (or outlet) inner wall. The pressure was computed at the location of these sensors, and then used to compute an estimate of the wavenumber spectrum component corresponding to a chosen axial wavenumber. That axial wavenumber will be referred to as the error wavenumber. Due to the limited number of sensors that could be realistically placed along the duct, the resolution of the calculated estimates of the wavenumber spectrum components was poor. As a result, when minimizing the estimate of a specific wavenumber component, a range of wavenumber components was actually minimized.

With this method, a single array of control sources was used to generate the control field. This technique was used in an attempt to reduce the sound power level within the 40° to 155° sector. Radiation from either the inlet or outlet of the duct was controlled by targeting either the positive or negative wavenumber components of the spectrum.

a) Control of the inlet radiation – pure active control

An axial array of four pressure sensors was used for this case. The sensors were placed along the duct inner wall between 1.55 m and 1.7 m with a spacing of 0.05 m. This configuration corresponds to a resolution of 41.8 m^{-1} for the computation of the components of the wavenumber spectrum. The reduction in sound power level that could be achieved in various sectors of the far field by targeting different error wavenumbers (i.e., by minimizing estimates of different components of the wavenumber spectrum), and for various locations of the control source array, was computed. The control source array was stepped throughout the inlet and outlet of the duct between –1.7 m and 1.5 m, with an increment of 0.1 m, while the values of the error wavenumbers targeted were varied between 5 m^{-1} and 29 m^{-1}. The results are presented in Figures 2.17(a), 2.17(b) and 2.17(c). It is observed that the reduction in sound power level that could be achieved in the different sectors of the far field shows no dependence with respect to which wavenumber component was being minimized. The levels of reduction were found to be sensitive only to the location of the control source array. Thus, with a resolution of 41.8 m^{-1}, the control system, although able to reduce sound power level, is unable to identify the different wavenumber components of the spectrum, and therefore is unable to target its control effort toward any specific region of the far field.

Increasing the number of pressure sensors from four to six, and changing the spacing between them to 0.1m improved the resolution to 12.56 m^{-1}. The optimization process of the control system was then repeated. The results are presented in Figures 2.18(a), 2.18(b) and 2.18(c). From these figures, it is seen that the level of reduction achieved in each sector varies with respect to the control source array location, as well as with respect to the error wavenumber. Thus, by increasing the resolution, the control system was able to better estimate, and therefore to better differentiate the components of the wavenumber spectrum. As a result, the control system could target specific sectors of the far field, increasing the reduction in each of them.

Thus, with a resolution of 41.8 m^{-1}, the control system was able to achieve a reduction in sound power level of up to 1.5 dB, 4.4 dB, 4.0 dB and 1.16 dB, respectively, for the (0°- 40°), (40°- 70°), (70°- 90°) and (40°- 155°) sectors, as compared to 1.8 dB, 5.2 dB, 4.6 dB and 2.3 dB, for the respective sectors, with a resolution of 12.5 m^{-1}. Therefore, by increasing the resolution, the ability of the control system to lock on to the propagating modes was improved.

Note from figures 2.18(a) and 2.18(b) that the best level of reduction that could be achieved in the target sector was of 2.3 dB when the control source array was located 0.25m upstream of the fan, and when the error wavenumber was comprised between 7 m^{-1} and 11 m^{-1}. This corresponds to the reduction that could be achieved with the fuselage error sensor technique using one control source array in the rigid wall case. However, in the fuselage sensors case, the optimum solution was not as sensitive to the location of the control source array as is in the present case. The possible levels of spillovers were also much less important. Thus, an increase in sound power level of only up to 4 dB because of spillover could occur within our target sector using the fuselage sensor technique, whereas with the error wavenumber technique spillovers of up to 26 dB could occur. With the fuselage error sensors technique, the modes that propagate within the target sector are targeted directly. This is not the case with the wavenumber technique, leaving therefore more room for errors. This could explain why the wavenumber sensor technique led to an optimum solution that was less robust, and why the control system was more prone to generate spillover.

Placing the control source array at its optimum location, the attenuation in sound pressure level that could be achieved in the far field of the inlet for different error wavenumbers was then computed. These results are presented in Figure 2.19. They do not show a very good correlation between the error wavenumber that was being targeted and the direction of the far field where reduction was achieved.

b) Control of the inlet radiation – hybrid control

Next, the effects of adding a liner to the active control system were studied. The duct was assumed to be lined over its entire length except at the tip of the inlet and outlet. This hybrid control system was optimized by looking for the error wavenumber, the control source array location, and the liner impedance that would lead to the maximum reduction in sound power level within the target sector. These three parameters where optimized simultaneously. The value of the error wavenumber was varied between 5 m^{-1} and 30 m^{-1} with an increment of 1 m^{-1}, while the axial location of the control source array was stepped along the duct length from 1.65 m downstream of the fan to 1.15 m upstream of the fan in 0.1 m increments. The specific resistance and reactance of the liner were varied between 0.1 and 5 for the resistance and between –3 and 3 for the reactance, both with an increment of 0.2.

The best attenuation that could be achieved in the target sector was 6.3 dB. This is an improvement of 4 dB over the pure active control case. This reduction in sound power

level was obtained for a liner of specific resistance 0.1 and specific reactance 0.7, for a target error wavenumber of 7 m^{-1}, and for a location of the control source array of 1.55 m downstream of the fan.

Placing the control source array at its optimum location, the attenuation in sound pressure level that could be achieved in the far field of the inlet for different error wavenumbers was then computed. This result is presented in Figure 2.20, and does show a good correlation between the error wavenumber that is being targeted and the direction of the far field toward which reduction is achieved. Thus, it can be seen that as the error wavenumber increases, the zones of the plot where reduction is achieved tilt toward the axis of the duct. In the rigid wall case, the wavenumbers of the modes that are propagating toward the inlet of the duct were (in increasing radial orders) 24.0 m^{-1}, 23.3 m^{-1}, 22.3 m^{-1}, 21.0 m^{-1}, 19.2 m^{-1} and 16.8 m^{-1}, while in this lined wall case, these wavenumbers are 23.7 m^{-1}, 22.9 m^{-1}, 21.8 m^{-1}, 20.4 m^{-1} and 18.5 m^{-1}. It is noted that the difference Δk_z between consecutive wavenumbers is, in average, larger in the lined wall case than in the rigid wall case. In the rigid wall case, Δk_z varied from 0.7 m^{-1} for the first two modes that were cut on, to 2.4 m^{-1} for the last 2 modes that were cut on, while in the lined wall case, Δk_z varies from 0.8 m^{-1} for the first two modes that are cut on, to 2.7 m^{-1} for the last 2 modes that are cut on. Therefore, the good correlation observed in the present case between the error wavenumber being minimized and the region of the far field where noise reduction is achieved could be due to the fact that the presence of the liner in the duct causes the wavenumber spectrum to "stretch", and thus allowing the control system to better differentiate between each component of the wavenumber spectrum.

The robustness of this optimum solution with respect to the error wavenumber and to the location of the control source array was investigated. While the specific impedance of the duct inner wall was set to its optimum value of 0.1+0.7i, the attenuation in sound power level that could be achieved in the target sector for various locations of the control source array and various error wavenumbers was computed. These results are presented in Figure 2.21(a). They show that although the optimum solution remained sensitive to the control source array location, a much larger number of control source array location that led to reduction in the target sector was obtained, as compared to the rigid wall case. Thus, the presence of the liner increased the robustness of the control system.

From Figure 2.21(a), it can also be observed that reduction in sound power level was achieved in the target sector for almost all possible locations of the control source array when the lower error wavenumbers were targeted. Therefore, the control system demonstrated the ability to identify the range of error wavenumbers which corresponded to the modes that radiate within the target sector, since targeting the lower error wavenumbers corresponds to targeting the higher order radial modes (which are the ones that radiate within the target sector).

The robustness of the optimum solution with respect to the liner impedance was then assessed. Fixing the error wavenumber and the axial location of the control source array to their optimum values (7 m^{-1} for the error wavenumber and -1.55 m for the axial

location of the control source array), the reduction in sound power level that could be achieved with this hybrid system was computed for various values of the liner specific impedance. These results are presented in Figure 2.21 (b) and indicate that the optimum solution is not very robust with respect to the liner impedance.

c) Control of the outlet radiation – hybrid control

Next, the level of reduction that could be achieved in the target sector when targeting the negative wavenumber components of the spectrum instead of the positive ones, was investigated. This means that the modes that were propagating through the outlet of the duct were targeted, instead of the modes that were propagating through the inlet of the duct. An axial array of 6 wavenumber sensors was placed in the duct outlet. The sensors were placed along the duct inner wall between -1.7 m and -1.2 m with a spacing of 0.1 m. The duct was considered to be lined (since this technique demonstrated poor performances with a rigid duct), and this hybrid control system was optimized. The combination of liner impedance, control array location, and error wavenumber that would lead to a maximum reduction in the target sector was determined. A maximum reduction of 5.94 dB could be achieved for a liner impedance of 0.8+1.1i, an error wavenumber of $-3\ m^{-1}$, and a location of the control source array of 1.55 m upstream of the fan.

Placing the control source array at its optimum location, the attenuation in sound pressure level that could be achieved in the far field of the inlet for different error wavenumbers was then computed. The results are presented in Figure 2.22. They show, again, a good correlation between the error wavenumber that is being targeted and the direction of the far field where reduction is achieved.

The level of reduction of 5.94 dB that was achieved within the target sector when controlling the negative wavenumber components is 0.36 dB less than what was obtained when the inlet wavenumber components were targeted. This difference in performance between the two approaches is probably due to the fact that, as it was observed earlier, controlling the modes that radiate through the inlet of the duct has more impact on the overall reduction achieved within the target sector than when controlling the modes that radiate through the outlet of the duct. However, this difference in performance is relatively small. This could be due to the fact that although the wavenumber resolution, which is determined by the number of pressure sensors and the spacing between each sensor, is the same for the inlet and outlet cases, the estimates of the negative wavenumber components can be expected to be better than the estimates of the positive ones, because the wavelengths of the modes travelling towards the outlet opening are longer than the ones corresponding to the modes travelling towards the inlet opening. For example, in the inlet the wavelength of the first mode being cut on is 0.26 m, and the wavelength of the last mode being cut on (i.e., the (4,5) mode) is 0.37 m. In the outlet the wavelength of the first mode being cut on is 0.44 m and the wavelength of the last mode being cut on (i.e., the (4,5) mode) is 0.88 m. Therefore, the sampling of the waves of longer wavelengths (i.e., of the waves travelling toward the outlet) is more thorough than the sampling of the waves of shorter wavelengths travelling toward the inlet. As a result,

the wavenumber sensors technique could be expected to work better when targeting the negative wavenumber versus the positive wavenumbers.

It was also observed that the value of optimum liner specific impedance is not the same for the cases where positive or negative error wavenumbers were minimized. This could be due to the fact that, even though the modes that radiate through the outlet of the duct do it so at the same angle with respect to the duct axis as the modes that radiate from the inlet of the duct, the wave fronts of the outlet and inlet modes do not hit the wall (or the liner) of the duct with the same angles. This difference in angle is caused by the presence of uniform flow: the inlet modes propagate with a smaller angle with respect to the duct axis than the outlet modes. Therefore, the optimum liner value should indeed be expected not to be the same for the inlet and outlet control cases.

Regarding the wavenumber sensors technique, it was observed that:

(i) The presence of the liner improved the correspondence between the error wavenumber being targeted and the far field region where noise reduction was achieved. It also increased the number of locations of the control source array that led to reduction in the target sector.

(ii) The hybrid system improves by 4 dB the reduction that could be achieved in the target sector compared to the pure active noise control system.

(iii) The optimum solution is sensitive to both the liner impedance and to the control source array location.

(iv) Similar levels of reduction were achieved when targeting positive or negative axial wavenumbers.

2.2.4 Summary:

A table summarizing the optimum levels of reduction that could be achieved for the target sector using the different control systems that were studied is presented in Figure 2.23:

A maximum reduction of 4.5 dB could be achieved by the pure passive control system. This was an improvement of about 2 dB over what could be achieved by the pure active control systems when a single array of control sources was used to generate the control field. However, the performance of the passive control system was matched or exceeded when two control source arrays were used by the active control systems.

The performances of the hybrid control systems were better by an average of 4 dB than the ones achieved by the pure active or pure passive control systems. The addition of a liner to the active control systems also improved the robustness of the optimum solutions.

Finally, the hybrid control system based on the fuselage error sensors technique performed better than the hybrid system that was based on the wavenumber sensors technique. The former was also found to have a more robust optimum solution and to be easier to optimize: with the wavenumber sensors technique three parameters have to be optimized simultaneously (control source array location, error wavenumber and liner impedance), versus two parameters with the fuselage error sensors technique (control source arrays locations and liner impedance).

2.3 Main conclusions:

A more advanced model of active noise control of fan noise for turbofan engines has been developed. This model was found to be fast and versatile.

It was determined that active noise control has the potential to reduce, over a relatively large sector, the fan noise radiated by an ultra high bypass turbofan engine.

It was observed that a hybrid control system can achieve significantly better levels of noise reduction than a pure passive or pure active control system, and that its optimum solution is more robust than the one achieved by a pure active control system .

It was found in the cases here that in general, active noise control with the fuselage error sensors works better than using inlet wavenumber sensors.

3. EXPERIMENTS ON THE JT15D TURBOFAN ENGINE

This section presents the experimental results for investigating the application of ANC techniques for reducing the inlet noise radiated by a JT15D turbofan jet engine with fuselage-mounted error sensors at Virginia Tech. In order to put the results obtained this year into perspective, a list of previous accomplishments is included. They include:

1) Compact and lightweight rare-earth compression driver control sources were developed and implemented.
2) Global attenuation was achieved with an optimized configuration using a single control source array and farfield sensors.
3) Control over a desired sector was shown to be achieved with a proper configuration of control sources and farfield error sensors.
4) The potential of inlet mounted error transducers was shown in conjunction with a model reference control approach which requires temporary use of farfield error sensors.
5) Multiple circumferential control source arrays were shown to improve attenuation and reduce sideline spillover effects, i.e., control higher order radial modes.
6) The combination of passive and active components on a hybrid inlet was shown to be an effective strategy for reducing jet inlet noise using farfield sensors. The active control system was not embedded in the liner.
7) The potential of an inlet mounted error sensing strategy using a wavenumber sensing technique was shown to be effective when used in conjunction with a

passive liner. Reduction over desired sectors can be obtained by observing and minimizing particular wavenumbers.

Further information concerning the previous results can be found in the references [1-6].

The research goals for this year are as follows:

1) To experimentally demonstrate active control with fuselage-mounted error sensors and control actuators mounted on a realistic compact inlet.
2) To combine active and passive control techniques together to create a hybrid passive-active compact inlet.

The many aspects of these objectives include:

1)The design of apparatus and procedures for the implementation of active noise control methods on a turbofan engine.
2)The construction of the necessary apparatus, including control hardware and software, the upkeep of the JT15D engine and test cell, and all components of the system.
3)The implementation of all components of the developed system to experimentally demonstrate active noise control on the running turbofan engine.

3.1 The JT15D engine, test cell, and fuselage section

The engine, test cell, and the components of the ANC system shown in will be discussed in the next sections. The engine used for this research project is a Pratt and Whitney JT15D-1 turbofan engine. It is a twin spool turbofan engine with a full length bypass duct and a maximum bypass ratio of 2.7. There is a single-stage axial flow fan with 28 blades and a centrifugal high pressure compressor with 16 full vanes and 16 splitter vanes. There are no inlet vanes and the diameter at the fan stage location is 0.53 m (20.8 in). All experimental results were obtained by operating the engine at idle condition which corresponds to a fan speed of approximately 5250 rpm, yielding a blade passage frequency (BPF) of approximately 2320 Hz. At this condition, the inlet intake flow speed is about 42.5 m/s which yields a Mach number of M=0.12. The engine is installed in a test cell configuration as shown in Figure 3.1. The engine is equipped with an inlet inflow control device (ICD) constructed at Virginia Tech from a NASA design. The purpose of the ICD is to minimize the spurious effects of ground testing on acoustic measurements by breaking up incoming vortices. The maximum diameter of the ICD is 2.1 times the engine inlet diameter. To enhance the tonal nature of the inlet radiated sound and to excite the m=1 mode to dominance, a set of 27 exciter rods are mounted upstream of the fan stage. The wake from the rods interact with the fan blades to produce tones which are significantly higher in sound level than without the rod interactions, and thus models strong wake-stator interactions. These rods extend 27% of the length of the fan blades through the outer casing into the flow and are placed in the inlet of the engine 10 cm (3.9 in) upstream of the fan stage.

The engine test cell consists of two chambers, with the forward section consisting of a semi-anechoic chamber to simulate free field conditions. One wall of the semi-anechoic chamber is open to the atmosphere for engine intake air. A simulated fuselage section was constructed with a wood frame and a thin aluminum skin and mounted near the top of the test cell as shown in Figure 3.1. The effective radius of the fuselage was 6 ft, with an overall length of 12 ft. The fuselage section was centered about the axis of the engine and mounted so that its surface was 56 inches above the top of the engine inlet. The microphone error sensors mounted in the fuselage will be explained in detail in section 3.6. Figure 3.2 is a picture taken from the front of the test cell showing the test cell, the fuselage section and the ICD.

3.2 The control algorithm

The control strategy is the feedforward Filtered-X LMS algorithm. In general, the algorithm generates the control input by filtering a reference signal which is coherent with the error signal (the signal to be cancelled) through an adaptive filter, before being input to the control actuators. More detailed information can be found in the references [1-5]. The results in this work were obtained with a multi-channel controller, allowing up to six inputs and six outputs (6I6O). The control algorithm was implemented on a TMS320C30 digital signal processing board hosted in a PC. The sampling frequency used in all experiments was 10000 Hz.

3.3 The compact hybrid passive-active inlet

In order to facilitate the rapid installation and removal of passive and active control components on the engine inlet, a compact hybrid inlet section, which allowed various configurations of both passive and active elements, was constructed. The hybrid inlet consists of a perforated mesh cylindrical skeleton, supported at each end by two circular plate rings and in the middle by four rectangular beams located geometrically 90° apart. The passive and active elements could then be mounted behind the mesh cylinder, which is acoustically transparent over the frequency range of interest. A rigid-wall inlet could be implemented by mounting sections of a hard, rigid material behind the mesh skeleton. The inner diameter of the inlet was 0.53 m (20.8 in) in order to match the diameter of the engine at the fan stage where the inlet was to be mounted. The length of the inlet in the axial direction was 0.46 m (18 in), including the two 6 mm (0.25 in) thick plate rings at each end of the inlet to allow attachment of the inlet to the engine at one end and the attachment of the ICD to the inlet at the other. A schematic of the compact inlet is shown in Figure 3.3.

3.4 The control actuators

The control actuators used in this research were developed at Virginia Tech for ANC on the JT15D engine. The diaphragms are commercially available 8 ohm elements with a voice coil diameter of 2.5 cm. In order to make the acoustic source as small and lightweight as possible, the speaker magnet element was designed and constructed with a neodymium iron-cobalt (rare-earth) magnet. Because of the high magnetic field generated by this material (about ten times of regular magnets), the size of the speaker motor can be significantly reduced while maintaining the output levels. The speaker assembly with the rare-earth magnet is 4.5 cm in diameter and 2.5 cm thick and weighs 257 g. This source has a fairly flat frequency response from 2 to 4 kHz, and was designed for cancellation of the BPF tone at 2300 Hz. This speaker motor is less than half the size and a third of the weight of the commercially available speaker motor designed for used with the same diaphragms.

A second set of acoustic sources shown were also made using neodymium magnets, but were designed with 5.1 cm (2 in) diameter voice coils and thus have a lower frequency range. These larger sources were designed for the NASA Lewis 4-foot diameter ducted fan with a tone at 1000 Hz [5], but generated enough sound levels at 2300 Hz so they could also be used on the JT15D engine.

The control signal(s) supplied to the group of drivers were phased in such a way as to generate a spinning mode of circumferential order m=1 in the duct inlet, i.e., since all twelve drivers were being driven by one control signal, then the phase delay between adjacent sources around the circumference was -30°. The phase delay between the sources in the control array were fixed with an analog phase-shifting circuit. The source magnitude and phase calibration is carried out for each source individually using a microphone located at 0° just beyond the ICD. Using a constant reference voltage signal (usually of 1.0 Volt) the power amplifier gain of each of the control drivers is adjusted individually so that all control sources generate the same level at the microphone located at 0°. The phase response (relative to the reference voltage signal) is measured and adjusted for each source individually as explained above to ensure the generation of the m=1 spinning modes.

The control signals were low pass filtered at 2500 Hz after being output from the controller board and before being input to the phase shifter and power amplifiers.

3.5 The reference sensor

The reference signal, required by the feedforward controller, is obtained by a proximity sensor mounted flush with the casing at the fan stage location. This eddy-current sensor picks up the passage of each of the fan blades and generates a sequence of pulses. By proper filtering, the output from this sensor provides a time histories highly correlated with the fan BPF and its harmonics. The reference signal is low-pass filtered at a cut-off frequency of 2500 Hz with a 48 dB/octave filter. The key feature of this

transducer is that it yields a non-acoustical signal, and will therefore not be affected by the action of the control input(s), i.e. no control feedback effects. This is a very important characteristic from the controller robustness point of view.

3.6 The error sensors and sensing strategies

The error signals to be minimized were supplied by pressure transducers mounted in the fuselage section shown in Figures 3.1 and 3.2. The pressure transducers were actually small, commercially-available neodymium speakers with a 5 cm (2 in) paper diaphragm. Twelve such sensors were mounted 30.5 cm (12 in) apart over the length of the fuselage at the closest point of the fuselage which corresponded to the axis of the engine (see Figures 3.1 and 3.2.) This spacing together with a distance of 1.42 m (56 in) from the top of the engine inlet resulted in the distances and angles shown in Table I for each of the error sensors with respect to the center of the inlet at the inlet opening. Proper selection of the error sensors was performed to select sectors for control.

Table I: Angle and distances of fuselage-mounted error sensors

Error #	Angle (°)	Distance (m)
1	104	1.78
2	94	1.73
3	84	1.74
4	74	1.80
5	65	1.90
6	57	2.05
7	51	2.23
8	45	2.43
9	41	2.66
10	37	2.90
11	33	3.14
12	30	3.40

3.7 Measurement facilities

The acoustic field of the JT15D engine is monitored with an array of 19 farfield microphones positioned in the horizontal plane passing through the centerline of the engine, and an array of 10 microphones positioned in the vertical plane. The microphones are spaced along an arc of radius 1.6 m (63 in) at 10° increments to obtain the acoustic directivity from -90° to 90° in the horizontal plane, (where 0° is along the engine axis) and from 0° to 90° in the vertical plane (towards the fuselage section). These microphones are used to evaluate the effects of the passive liner and the ANC system on the noise radiated by the engine. The picture in Figure 3.2 also shows the two microphone array arcs with respect to the engine with the ICD installed. Spectrum

averaging of the microphone data was performed with a Bruel & Kjaer type 2032 spectrum analyzer.

3.8 Control using a 1C4E control system

The first results presented will be those achieved using one control array located at x_{c1} = 0.3 m (see Figure 3.3 for coordinate origin) and the four error sensors located at θ = 45°, θ = 57°, θ = 65°, and θ = 74°. The control sources used were the larger ones with a voice coil diameter of 2 inches. The directivities of the BPF tone at a frequency of 2328 Hz for the inlet configured as a rigid wall, the inlet configured with a passive liner, and for the inlet with both passive and active noise control are shown in Figures 3.4(a) and 3.4(b) in the horizontal and vertical planes, respectively. It is clear that minimizing the BPF at angles in the "upward" direction (i.e., toward the fuselage) also results in reduction at similar angles in the horizontal plane as well. It is extrapolated that the region of achieved reduction is symmetric about the axis of the engine even thought the tone is only minimized in one direction. Thus the area of reduction seems to exist as a sector of rotation about the engine axis as is predicted analytically and expected due to the symmetric nature of the radiated noise about the azimuth of the engine. In this experiment, reduction beyond the passive-only case (which in all experiments represents a "before control" directivity) is evident over the sector from approximately 40° to 60° in the farfield. Some spillover is observed mainly toward the engine axis at the angles of 30° and 40°. The additional power reduction of the BPF tone obtained with active control over the passive only case for the total and two different sectors are tabulated in Figure 3.4(c). The total power was actually increased after control due to the spillover toward the front of the engine. The power reduction obtained over the two sideline sectors shown in the table were less than 2 dB with this configuration.

3.9 Results using a 2C4E control system

The next results are for a configuration using two control arrays, the first array (with the large sources) was located at x_{c1} = 0.3 m, and the second array (with the small sources) was located at x_{c2} = 0.48 m (again refer to Figure 3.2 for the coordinate origin.) The four error sensors minimized were located at θ = 40°, θ = 45°, θ = 50°, and θ = 57°. The directivities of the BPF tone at a frequency of 2328 Hz for the inlet configured as a rigid wall, the inlet configured with a passive liner, and for the inlet with both passive and active noise control are shown in Figures 3.5(a) and 3.5(b) in the horizontal and vertical planes, respectively. A significant improvement in the BPF tone reduction is evident with the addition of a second control array and a slightly different error sensor selection. Reductions of the BPF tone level approach 10 dB at some angles with very little control spillover. The additional power reductions in the BPF tone achieved by the active control system beyond the passive-only case are shown in the table of Figure 3.5(c). A total power reduction of 1.8 dB is now evident with reductions over the sideline sectors exceeding 4 dB.

3.10 Results using a 2C2E control system

The results for the best case of active noise control with fuselage error sensors are shown in Figure 3.6. This experiment used a 2C2E system with x_{c1} = 0.3 m, and the x_{c2} = 0.48 m (the same control configuration as the last experiment.) Two error sensors were minimized located at θ = 57° and θ = 65°. Figures 3.6(a) and (b) show the radiation directivities in the horizontal and vertical planes, respectively. Global control is obtained over the entire directivity field with respect to the passive-only directivity. Reductions of up to 15 dB are obtained in some directions, with the most significant reductions occurring toward the larger angles, i.e., toward the engine sidelines. Again the total power reduction in the BPF tone and the power reduction over the sideline sectors are shown in the table of Figure 3.6(c) and show improvement over the previous experiment. It is clear from these experiments that significant reductions can be achieved with a control system with properly configured sensors and actuators.

3.11 Comparison of results using fuselage-mounted error sensors to those using wavenumber sensing

To evaluate the results achieved with ANC using fuselage-mounted error sensors, a comparison to the results previously obtained with ANC using the wavenumber sensing technique is in order. The results presented here using the wavenumber sensing technique were obtained during the research performed in 1997, and more detail can be found in the reference [6]. The wavenumber error sensing technique involves using conditioned signals from an array of inlet microphones to observe an axial wavenumber component propagating out of the engine inlet. The 1C1E controller is then used to minimize the signal from the wavenumber sensor. Figure 3.7(a) shows the SPL reductions over the horizontal directivity field as a function of the wavenumber minimized that was achieved with a single control source array located at x_c = 0.30 m embedded within a passively-lined inlet. It is clear in this figure that a trend exists between the sector over which reduction is achieved and the wavenumber minimized. Controlling lower wavenumbers tends to result in reduction towards the sideline sectors, and as the wavenumber minimized increases, the angle of reduction moves closer toward the engine axis. Thus with the passively-lined duct, it was shown that minimizing different wavenumbers corresponds to minimizing the radiation towards different angles in the farfield.

A similar plot is contained in Figure 3.7(b) for ANC with fuselage-mounted error sensors, which shows the SPL reduction over the horizontal directivity field plotted versus the angles of the pair of fuselage-mounted error transducers that were minimized. For the FES experimental results shown in Figure 3.7(b), a 1C2E controller was used with the same location of the single control array as was used in the wavenumber sensing case (x_c = 0.30 m) on a passively-lined inlet. The results with the fuselage error sensors show a similar and obvious trend that the sector of reduction occurs in the vicinity of the angles where the sensors are located. Due to the distance of the fuselage from the engine,

the smallest angle at which an error sensor could be located was 30°, thus the two plots do not correspond directly, as the rightmost case using the FES (with angles at 41° and 30°) shows a similar sector of reduction as that achieved by minimizing a wavenumber of about 15 m^{-1}.

Figure 3.8 contains a comparison between a 1C1E system with a single fuselage error sensor located at $\theta = 51°$ and a 1C1E system with the wavenumber sensing technique minimizing a wavenumber of k_x=5.2 m^{-1}. In both cases the single control array was located at $x_c = 0.30$ m, and embedded within a passively-lined inlet. The horizontal radiation directivities for minimizing the fuselage error sensor at $\theta = 51°$ and minimizing the wavenumber k_x=5.2 m^{-1} are shown in Figures 3.8(a) and 3.8(b) respectively. The control system with the single fuselage error sensor results in a significant notch near the angle where the error sensor was located in this case, with reductions exceeding 10 dB, while this case using the wavenumber sensing technique results in a more distributed region of reduction. The additional power reductions in the BPF tone for both cases are tabulated in the table of Figure 3.8(c) for the total and two sideline sectors. Thus, FES can be used to "notch the BPF tone in a particular direction

An additional comparison can be drawn between the previous wavenumber sensor experimental results with a 1C1E system shown in Figure 3.8(a) and results obtained with the 2C2E fuselage error sensing system as shown in Figures 3.6(a). The results for these two cases are comparable in terms of BPF total power reduction and power reduction over sectors. It should also be noted that the second control array for use with the fuselage error sensing technique was located in the axial location of the inlet where the inlet wavenumber sensors were located. Thus the fuselage error sensing technique produces a comparable reduction in the BPF tone as that achieved with the wavenumber sensing technique.

3.12 Effect of boundary layer noise

An issue that may potentially present a practical problem for the use of fuselage-mounted error transducers is the corruption of the error signals with induced boundary layer noise during flight. In 1971, Bhat published work regarding the results obtained with arrays of microphones flush-mounted on the skin of a Boeing model 737 fuselage both forward and aft of the wing-mounted turbofan engines. [7] In this paper it is reported that the prevalence of the engine tonal noise in the fuselage-mounted microphones depends on the flight Mach number. For M=0.78, the engine noise was completely masked by the boundary layer noise in the time domain; at M=0.6 the engine noise (i.e., the BPF at 3355 Hz) stood 1.5 dB above the broadband boundary layer noise; and at M=0.45 the BPF tones stood well above the broadband between 2 and 10 kHz. [7] These results imply that the fuselage sensing technique could work well with proper band pass filtering of the error signal, especially since the flight Mach numbers of the airplanes when they are near the ground (i.e., during takeoff and landing) when ANC is expected to be necessary are relatively low (e.g., M=0.3) and the boundary layer noise is not expected to be detrimental.

In order to investigate the effect of induced boundary layer noise into a fuselage mounted error signal, experiments were run on the JT15D engine with external uncorrelated random noise content added to the error signals before they were introduced into the controller. The experimental results presented here are for a 1C1E control system with the single control array located at $x_c = 0.3$ m, and for the single error sensor at $\theta = 57°$. First, the error signal was minimized by the controller without the addition of random noise, and the resulting before and after control spectra of the error signal are shown in the top plot of Figure 3.9(b). Before control, the BPF tone stood about 20 dB above the broadband noise level in the vicinity of the tone, and the controller reduced the BPF tone by 11.5 dB. The resulting radiation directivities for the rigid wall case, the passive control only case (i.e., the before control case) and the passive-active control case with no additional boundary layer noise (BLN) are shown in Figure 3.9(a). The controlled directivity shows reductions of up to 10 dB over the sector from about 50° to 70°, and the BPF power reductions are tabulated in Figure 3.9(c). Next, white noise was added to the error signal until the BPF tone stood only approximately 1.5 dB above the broadband noise, and the controller was converged (from its initial zero state) to minimize the new error signal corrupted with the simulated boundary layer noise. The error signal spectra with the simulated boundary layer noise before and after control are contained in the bottom plot of Figure 3.9(b), which shows that the error signal content at the BPF tone was reduced to the broadband background with control. The resulting directivity for this passive-active case with the addition of simulated BLN is also plotted in Figure 3.9(a). It is clear that a few dB of reduction were lost when the error signal contained BLN, and the BPF power reductions are tabulated in Figure 3.9(c). With the addition of BLN to the single error signal, 0.6 dB more spillover in the total BPF reduction was observed, and the BPF reductions over the sideline sectors from 50° to 70° and from 50°to 90° were reduced by 1.3 and 1.1 dB, respectively. However, the BPF tone standing only 1.5 dB above the broadband is considered to represent an extreme case of error signal corruption, and the fact that the control system still performed adequately shows that the influence of boundary layer noise should not be considered detrimental to the performance of the ANC system.

4. CONCLUSIONS

The following conclusions can be made concerning the research performed in this work:

1) The use of fuselage-mounted error transducers for use in conjunction with active noise control was experimentally shown to be an effective strategy for reducing the noise radiated at the BPF tone from turbofan engines. Reductions of the BPF radiated power of up to5.0 dB were obtained over the sector from 50° to 90°.
2) Proper selection of error signals and control actuator locations can result in selective control over sectors, and good control with only a small number of sensors and actuators.

3) The results with fuselage mounted error sensors are comparable to those obtained previously with the wavenumber sensing technique, and the fuselage error sensors provide the added advantage of using less inlet space.
4) The presence of boundary layer noise on the error signals is not expected to be detrimental to the performance of the ANC system.

5. ACKNOWLEDGEMENTS

This work was supported by the Aeroacoustics Branch of the NASA Langley Research Center which is gratefully acknowledged. The technical monitors for this work are Carl Gerhold and Joe Posey.

6. REFERENCES:

[1] Thomas, R. H., Burdisso, R. A., Fuller, C. R., and O'Brien, W. F., "Active Control of Fan Noise from a Turbofan Engine," AIAA paper 94-0361, 32nd Aerospace Science Meeting & Exhibit, Reno, Nevada, January 11-14, 1993.

2. Burdisso, R. A., Thomas, R. H., Fuller, C. R., and O'Brien, W. F., "Active Control of Spinning Modes from a Turbofan Engine," AIAA Journal, Vol. 32, No. 1, pp.23-30, 1994.

3. Burdisso, R.A., Fuller, C.R., Smith, J.P., "Experiments on the Active Control of a Turbofan Inlet Noise using Compact, Lightweight Inlet Control and Error Transducers," CEAS/AIAA-95-028, 1995, pp. 177-185.

4. Smith, J.P., Burdisso, R.A., and Fuller, C.R., Experiments on the Active Control of Inlet Noise From a Turbofan Jet Engine Using Multiple Circumferential Control Arrays, AIAA 96-1792, 1996.

5. Smith, J.P., Burdisso, R.A., "Active Control of Inlet Noise at the NASA Lewis Ducted Fan Facility," Virginia Tech Report VPI - ENGR.97.477, November, 1997.

6. Smith, J.P., Burdisso, R.A., "Active Control of Inlet Noise on the JT15D Turbofan Engine," Virginia Tech Report VPI - ENGR.97.263, December, 1997.

7. Bhat, W. V., "Flight test measurement of exterior turbulent boundary layer pressure fluctuations on Boeing model 737 airplane," J.Sound Vib. 14 (4), 439-457, 1971.

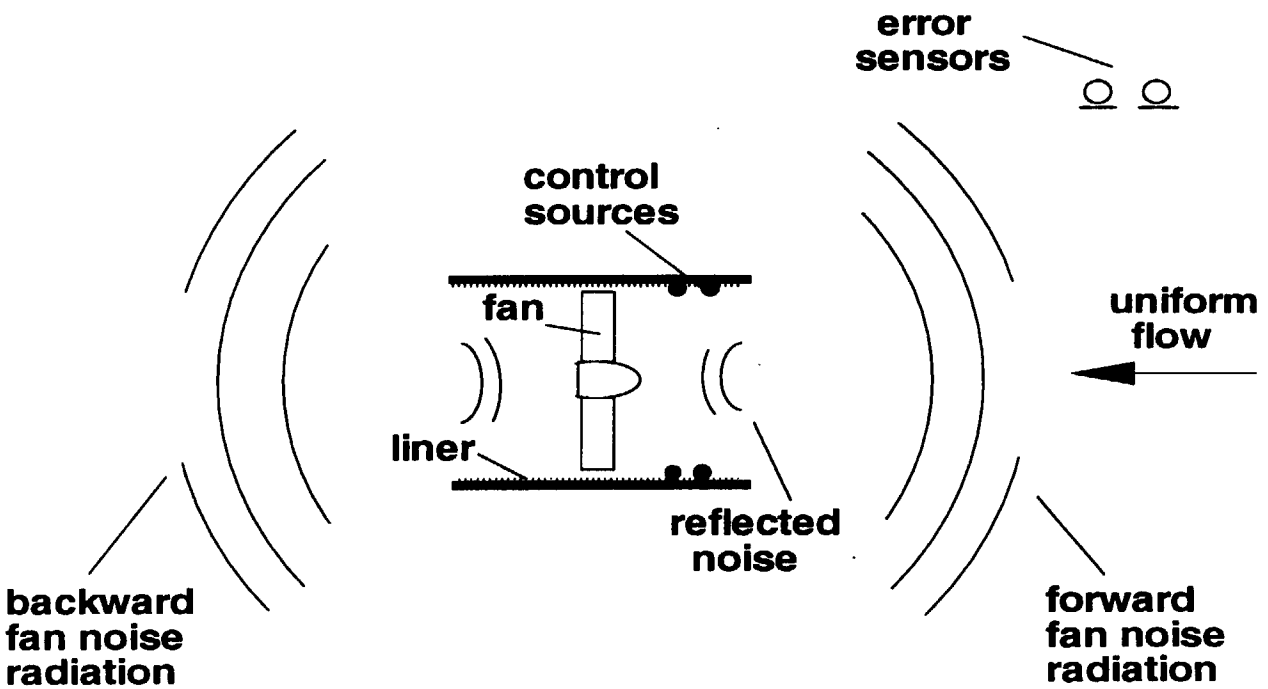

Figure 2.1: Schematic of the model

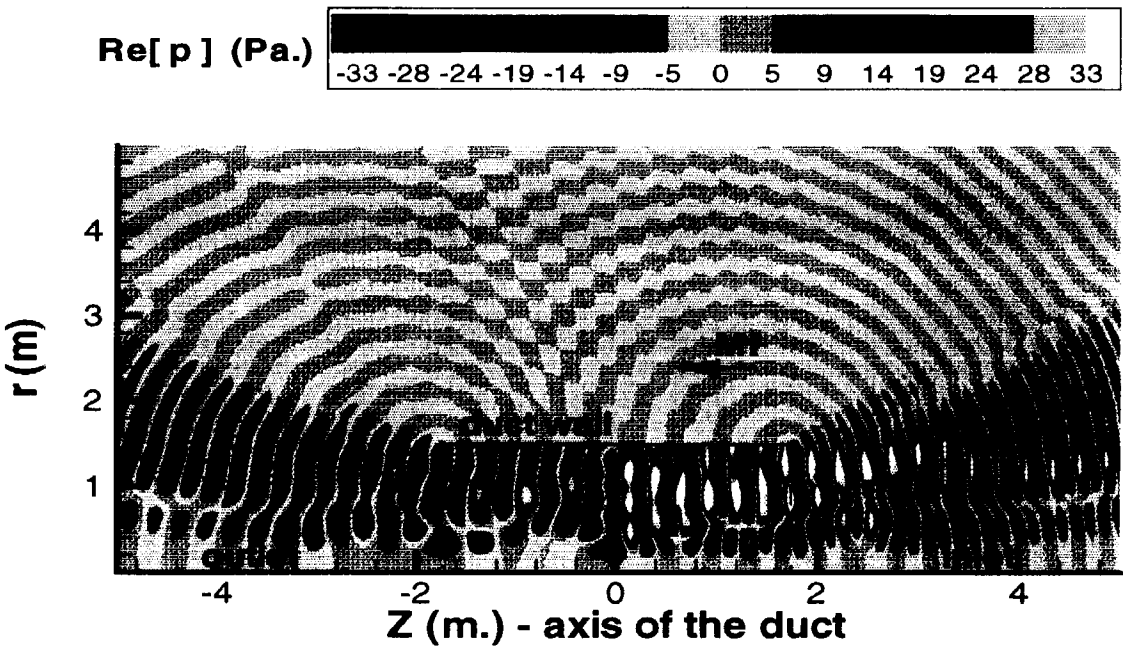

Figure 2.2: Pressure field. BPF=1000 Hz, Mf=0.25 and m=4

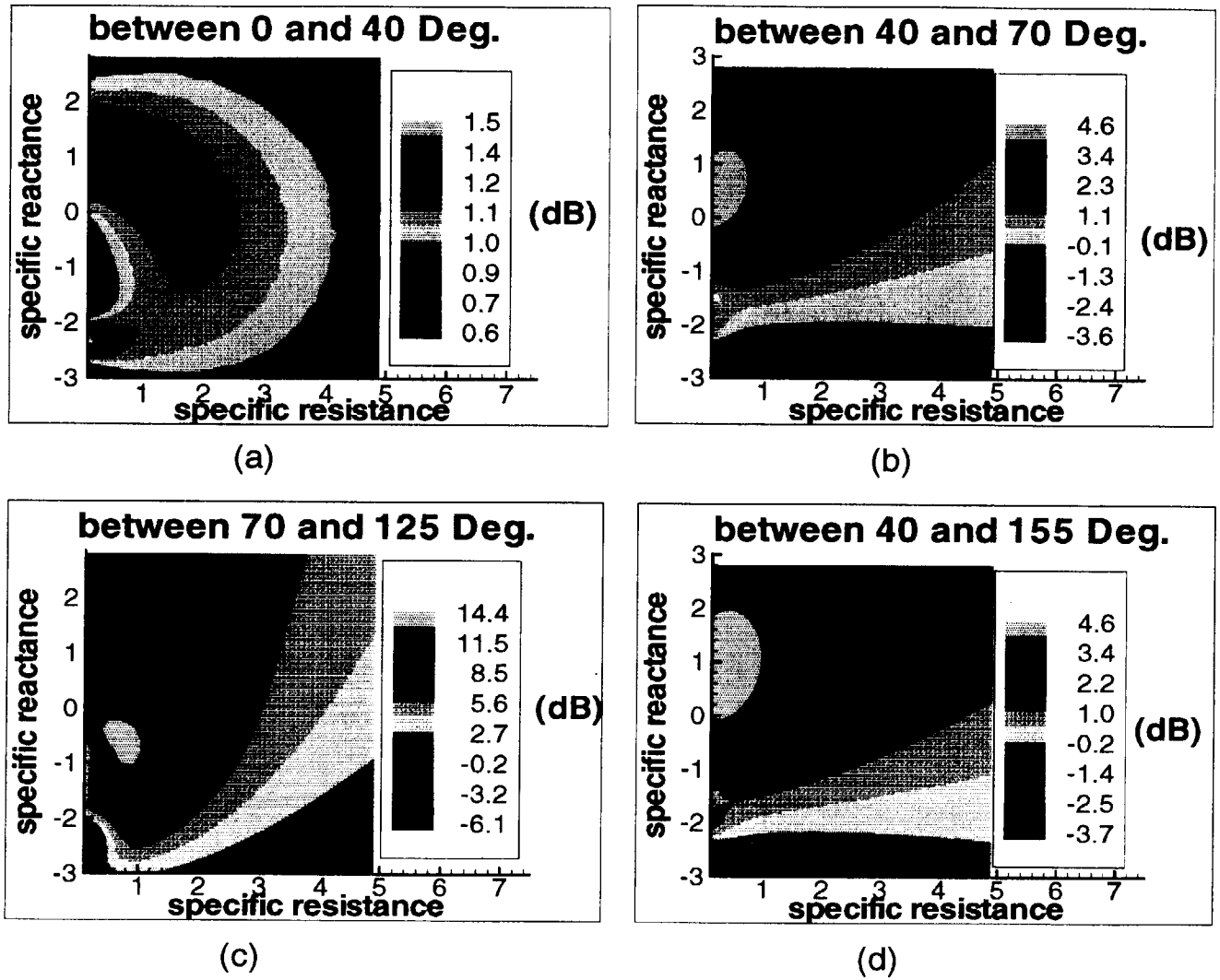

Figure 2.3: Attenuation in sound power level achieved in different sectors of the far field using a purely passive control system. Duct lined between -1.73 m and 1.73 m.

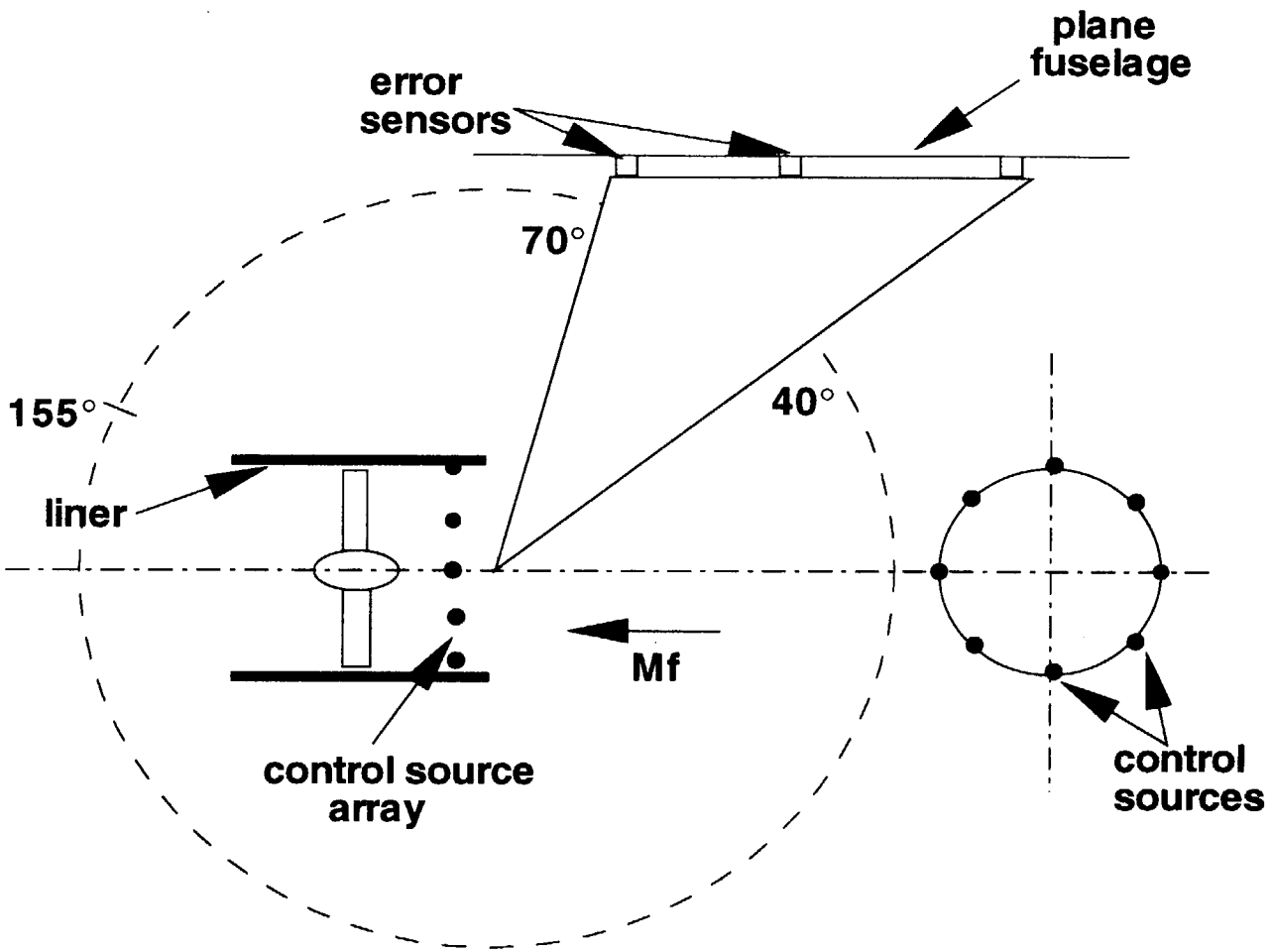

Figure 2.4: Schematic of the control system for the fuselage error sensors technique.

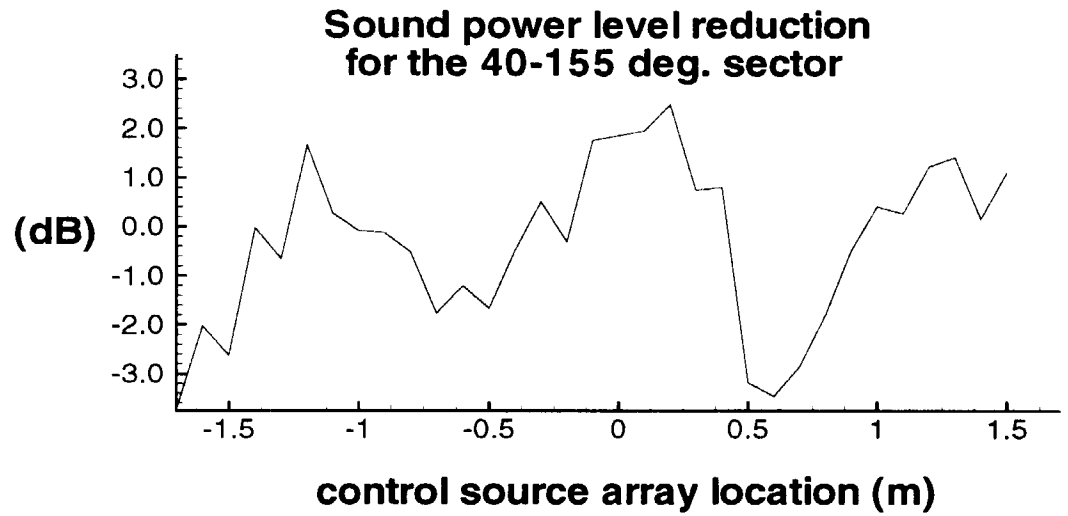

(a)

sector (deg.)	0-40	40-70	70-125	125-155	155-180	40-155
reduction (dB)	-0.43	3.36	3.2	0.2	-8.2	2.5
(max.)	0.3	3.75	0.9	-4.8	-7.9	0.74

(b)

Figure 2.5: Reduction in sound power level achieved in the target sector with the fuselage sensor technique. Pure ANC, 1 control source array and 3 error sensors within the 40-70 deg. sector. (a) all control source array locations, (b) optimum cases.

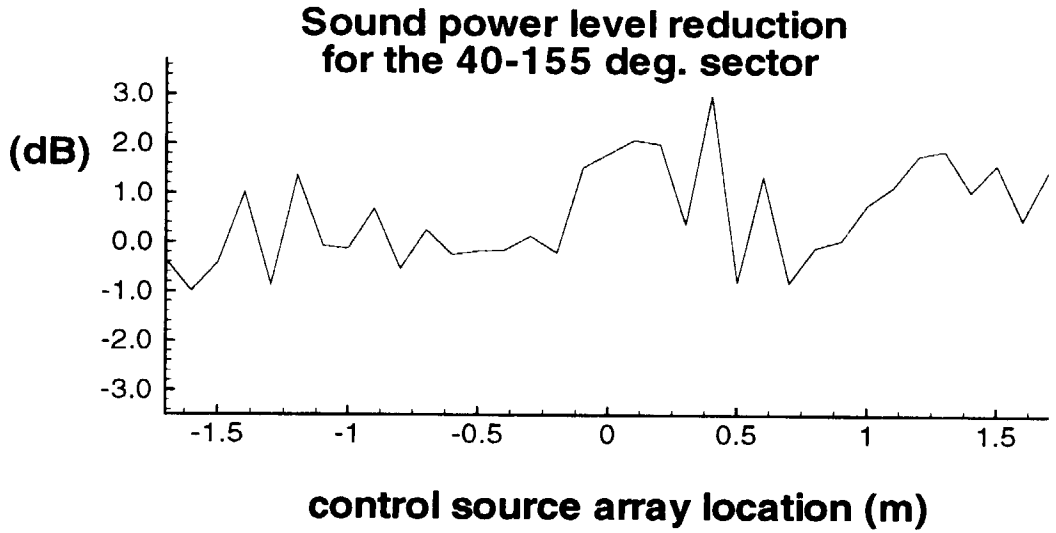

(a)

sector (deg.)	0-40	40-70	70-125	125-155	155-180	40-155
reduction (dB)	0.3	2.6	7.4	4.2	-7.1	2.9
(max.)	-0.23	4.41	-0.6	-5.6	-9.59	0.37

(b)

Figure 2.6: Reduction in sound power level achieved in the target sector with the fuselage sensor technique. Pure ANC, 1 control source array and 7 error sensors within the 40-70 deg. sector. (a) all control source array locations, (b) optimum cases.

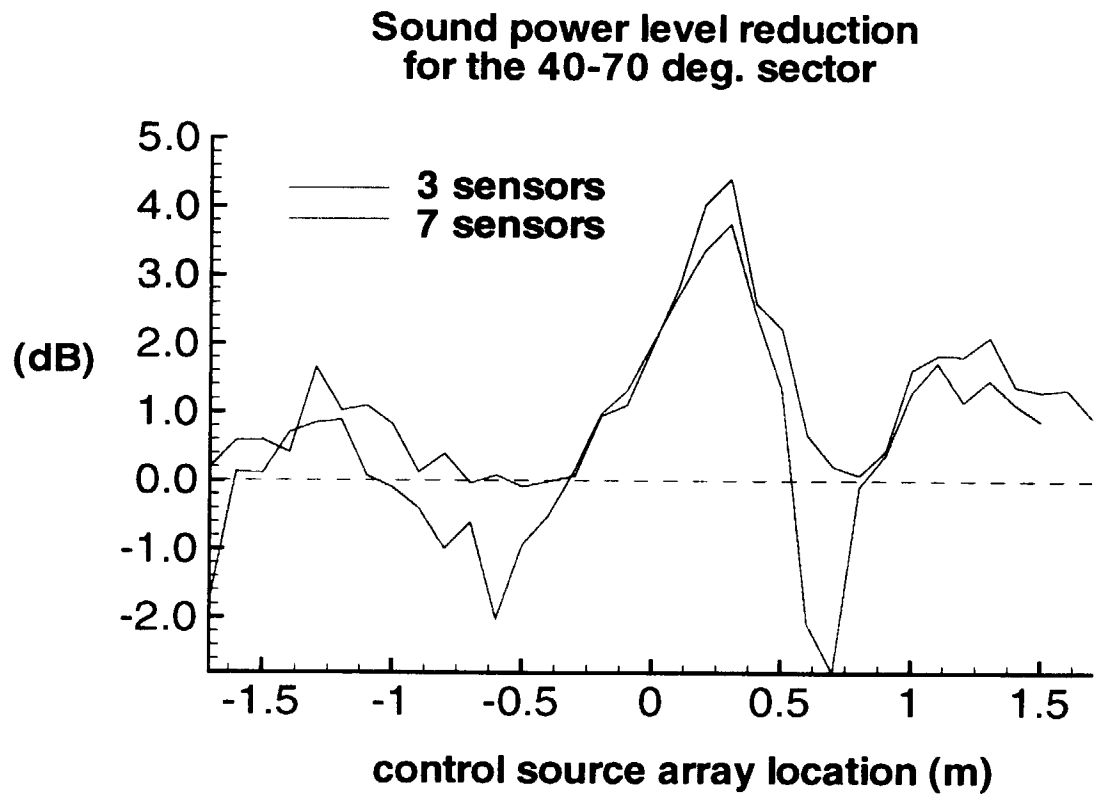

Figure 2.7: Reduction in sound power level for the 40-70 deg. sector with the fuselage sensors technique. Pure ANC. 1 control source array.

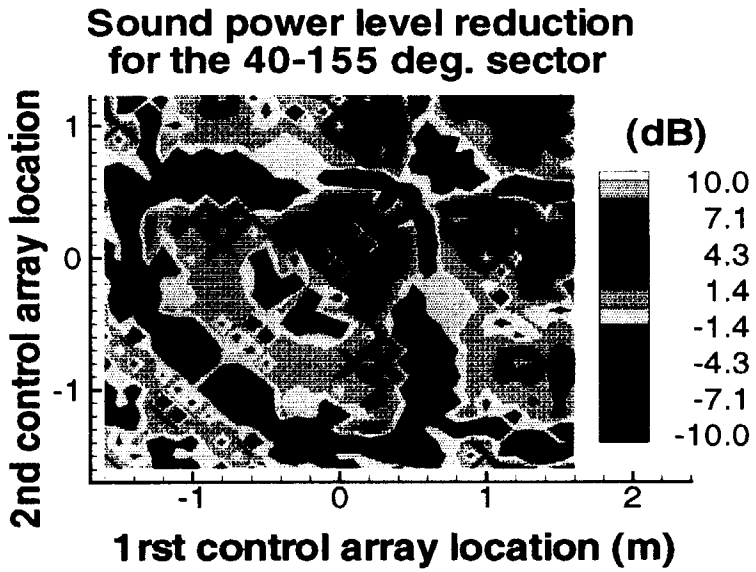

(a)

For the optimum configuration :

sector (deg.)	0-40	40-70	70-125	125-155	155-180	40-155
reduction (dB)	0.44	5.2	7.5	4.8	6.1	5.3

(b)

Figure 2.8: Sound power level reduction (a) for the target sector, (b) for the optimum case with the fuselage error sensor technique. Pure ANC, 2 control arrays and 3 sensors within the 40-70 deg. sector.

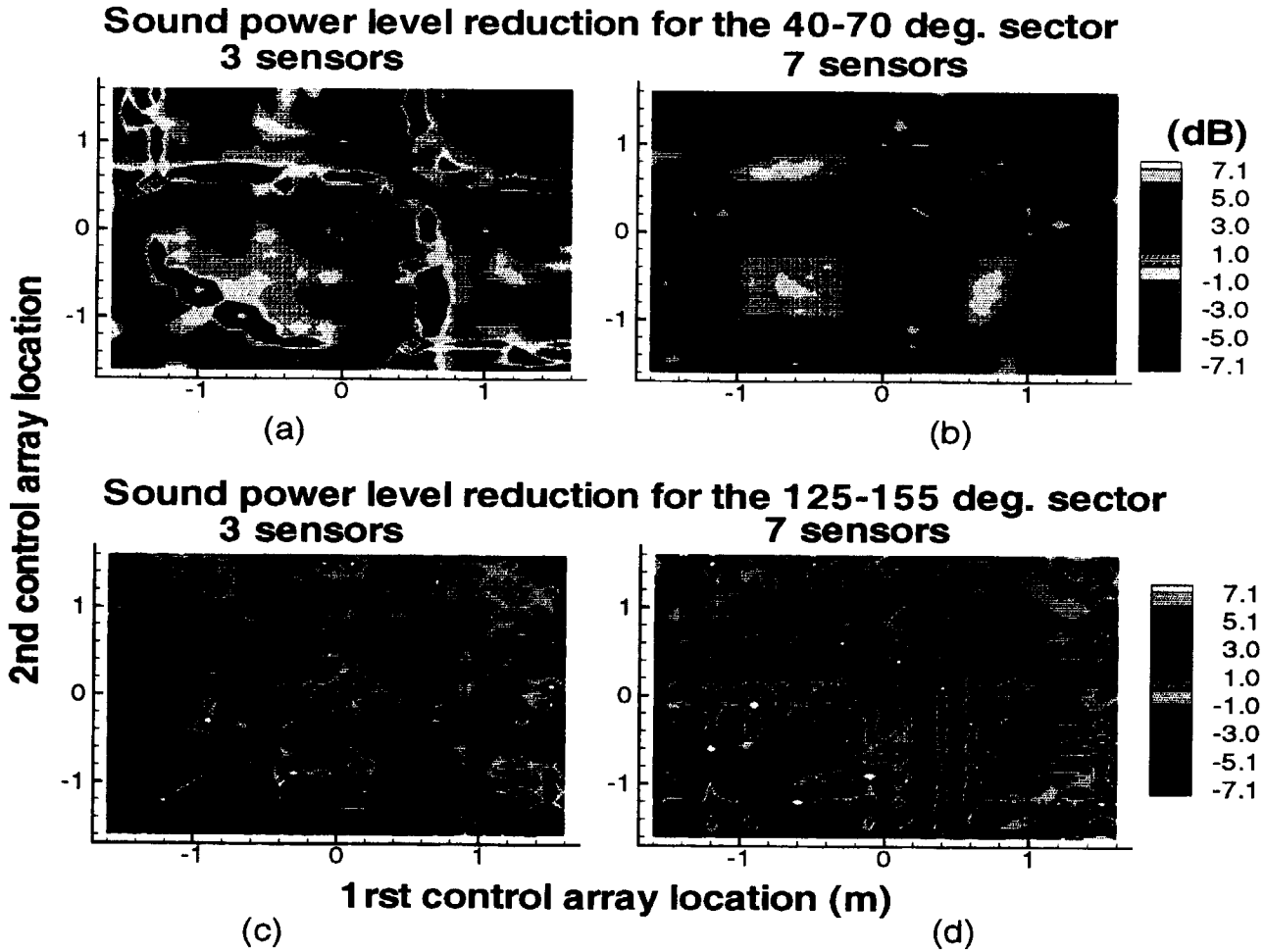

Figure 2.9: Sound power level reduction for the 40-70 deg. sector using (a) 3 error sensors, (b) 7 error sensors, and for the 125-155 deg. sector using (c) 3 error sensors, (d) 7 error sensors. Fuselage sensors technique. Pure ANC, 2 control source arrays.

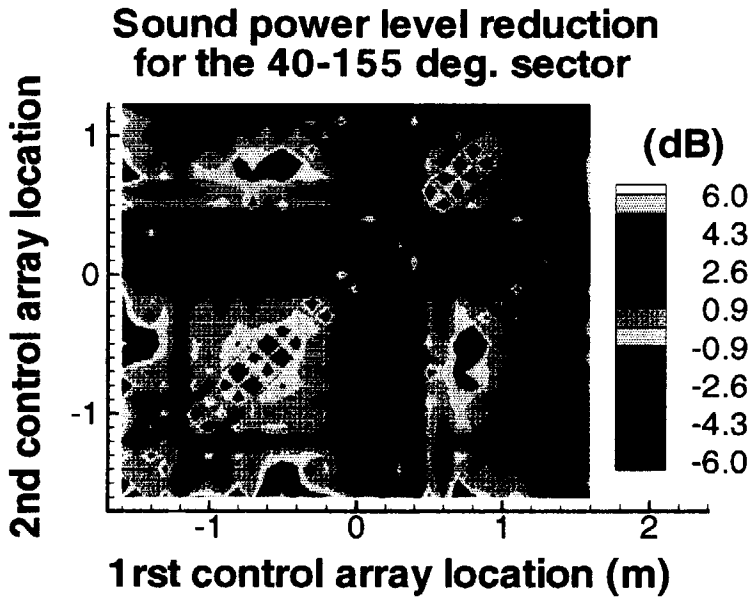

(a)

For the optimum configuration :

sector (deg.)	0-40	40-70	70-125	125-155	155-180	40-155
reduction (dB)	0.41	5.8	6.6	5.6	6.2	6.0

(b)

Figure 2.10: Sound power level reduction for (a) the target sector, (b) the optimum case with the fuselage sensors technique. Pure ANC, 2 control arrays and 7 sensors within the 40-70 deg. sector.

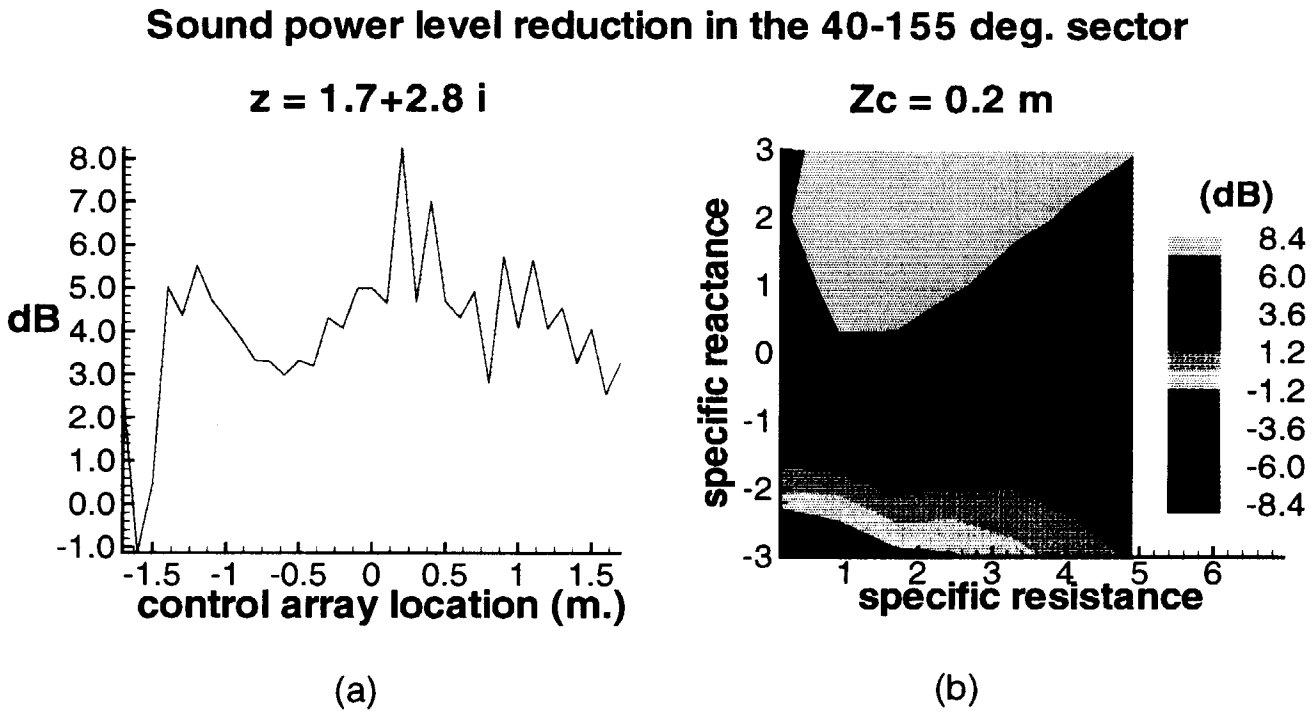

Figure 2.11: Sound power level reduction for the target sector (a) optimum liner impedance, (b) optimum control array location. Fuselage sensors technique. Hybrid control, 1 control source array and 3 error sensors.

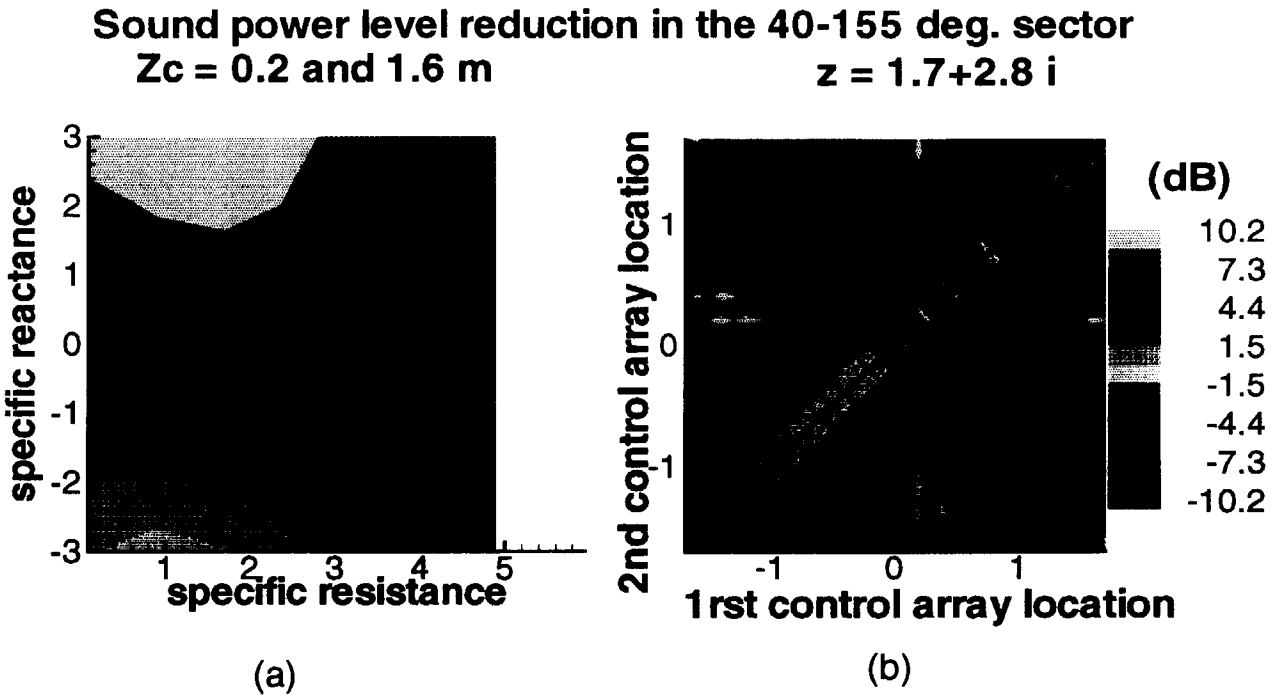

Figure 2.12: Sound power level reduction for the target sector (a) optimum control arrays locations, (b) optimum liner impedance. Fuselage sensors technique. Hybrid control, 2 control source arrays and 7 error sensors.

maximum reduction in SPWL for the 40-155° sector (dB) :

pure ANC		hybrid control	
1 control array	2 control arrays	1 control array	2 control arrays
2.03	4.3	7.3	9.6

with sensors within the 40-70 and 125-155 deg. sectors

(a)

2.5	6.0	8.4	10.2

with sensors within the 40-70 deg. sector only

(b)

Figure 2.13: Maximum reduction in sound power level for the target sector with the fuselage sensor technique (a) error sensors in the far field of the inlet and outlet, (b) error sensors in the far field of the outlet.

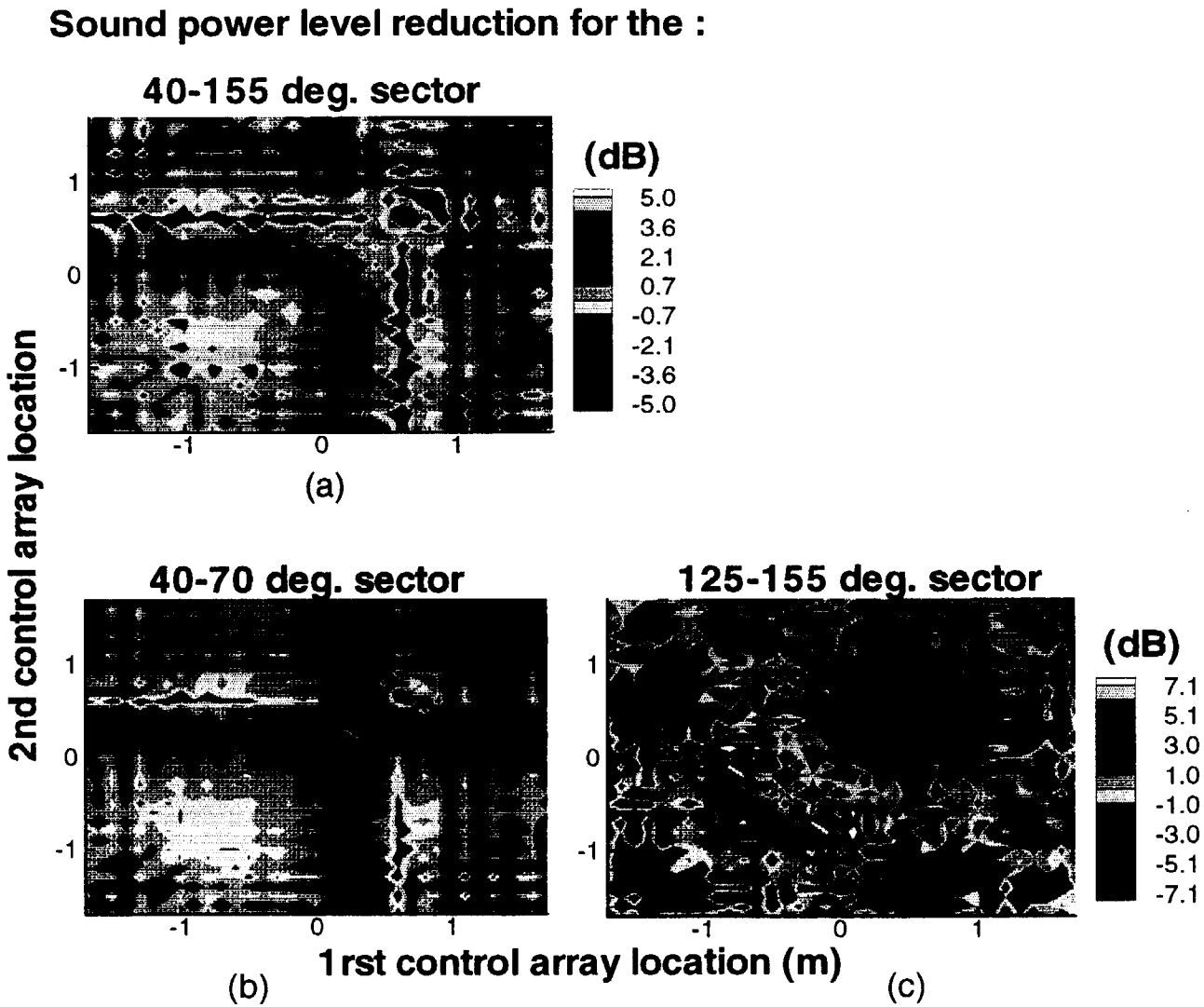

Figure 2.14: Sound power level reduction for the (a) target sector, (b) 40-70 deg. sector, (c) 125-155 deg. sector with the fuselage sensor technique. Control of inlet and outlet radiation. Pure ANC, 2 control source arrays.

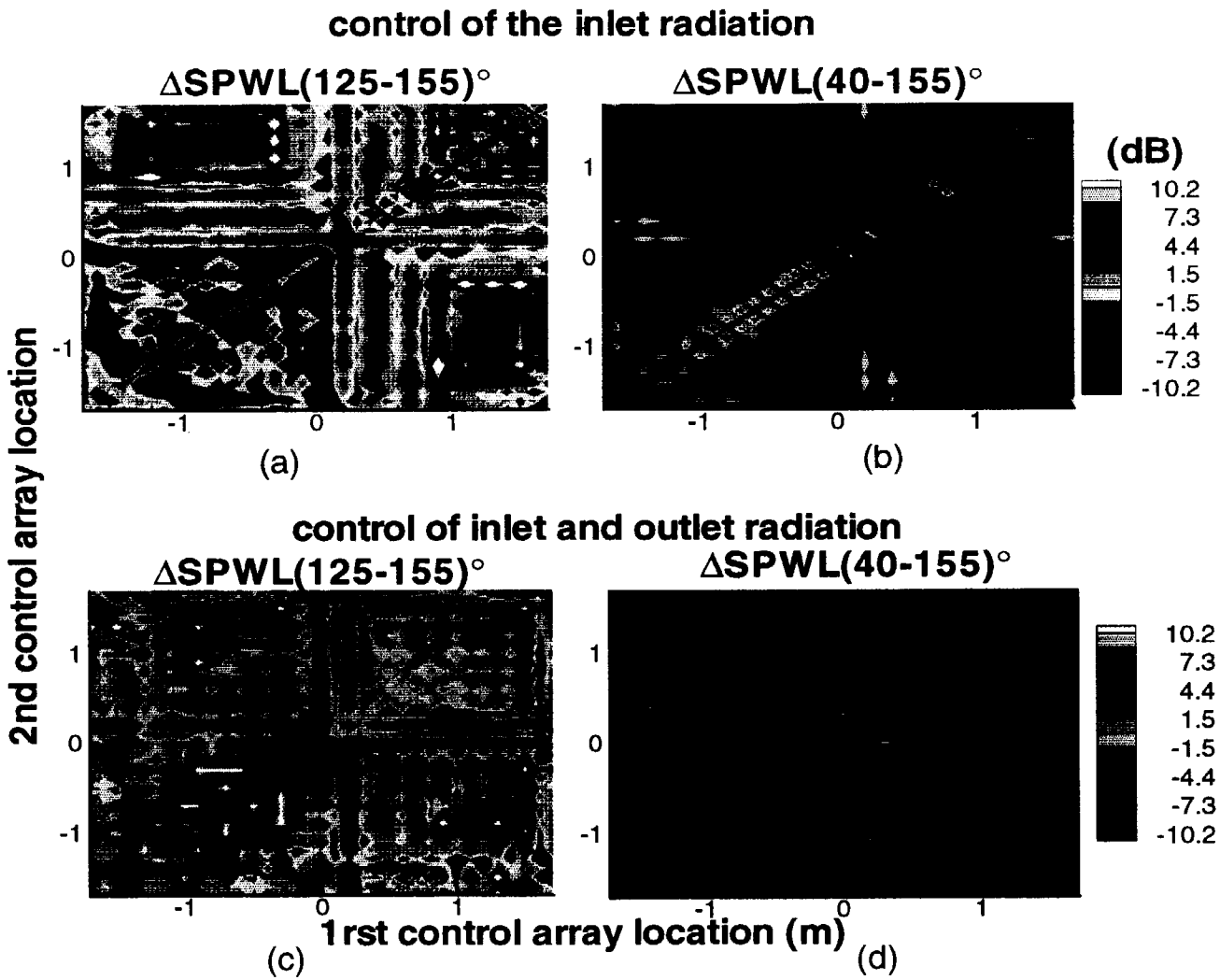

Figure 2.15: Reduction in sound power level with control of inlet radiation (a) for the 125-155 deg. sector, (b) for the target sector, and with control of inlet and outlet radiation (c) for the 125-155 deg. sector, (d) for the target sector. Fuselage sensors technique, optimum liner, 2 control source arrays.

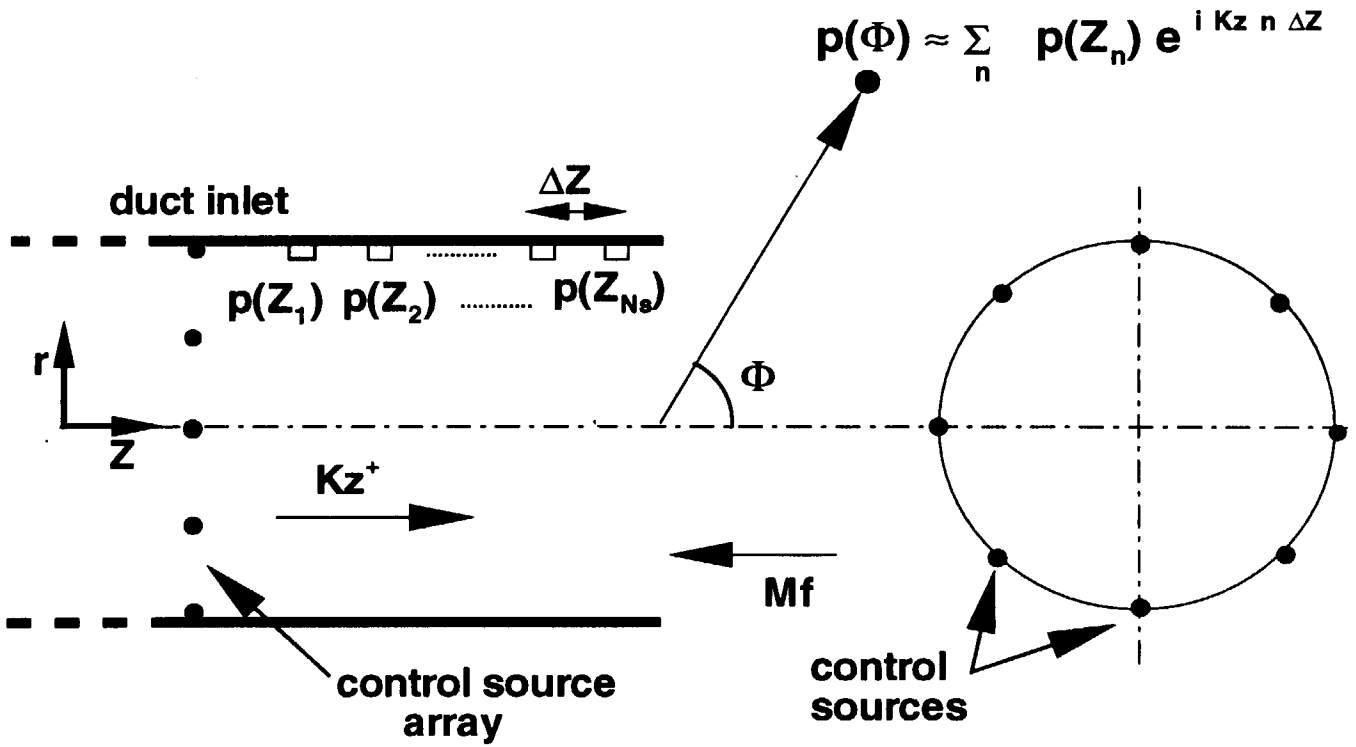

Figure 2.16: System schematic for the wavenumber sensors technique.

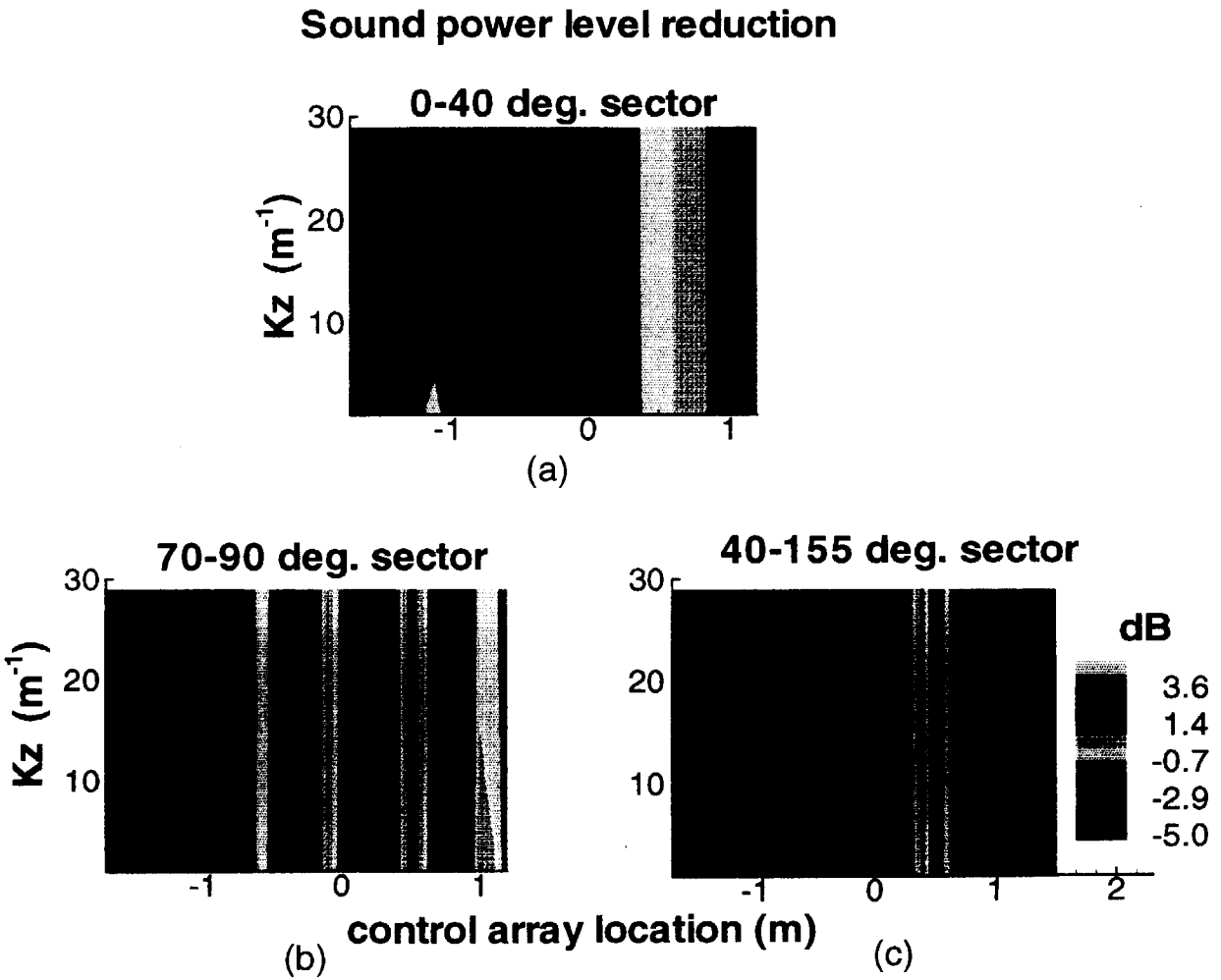

Figure 2.17: Sound power level reduction for the (a) 0-40 deg. sector, (b) 70-90 deg. sector, (c) target sector using the wavenumber technique. Pure ANC, 4 inlet sensors, resolution= 41.8 m^{-1}.

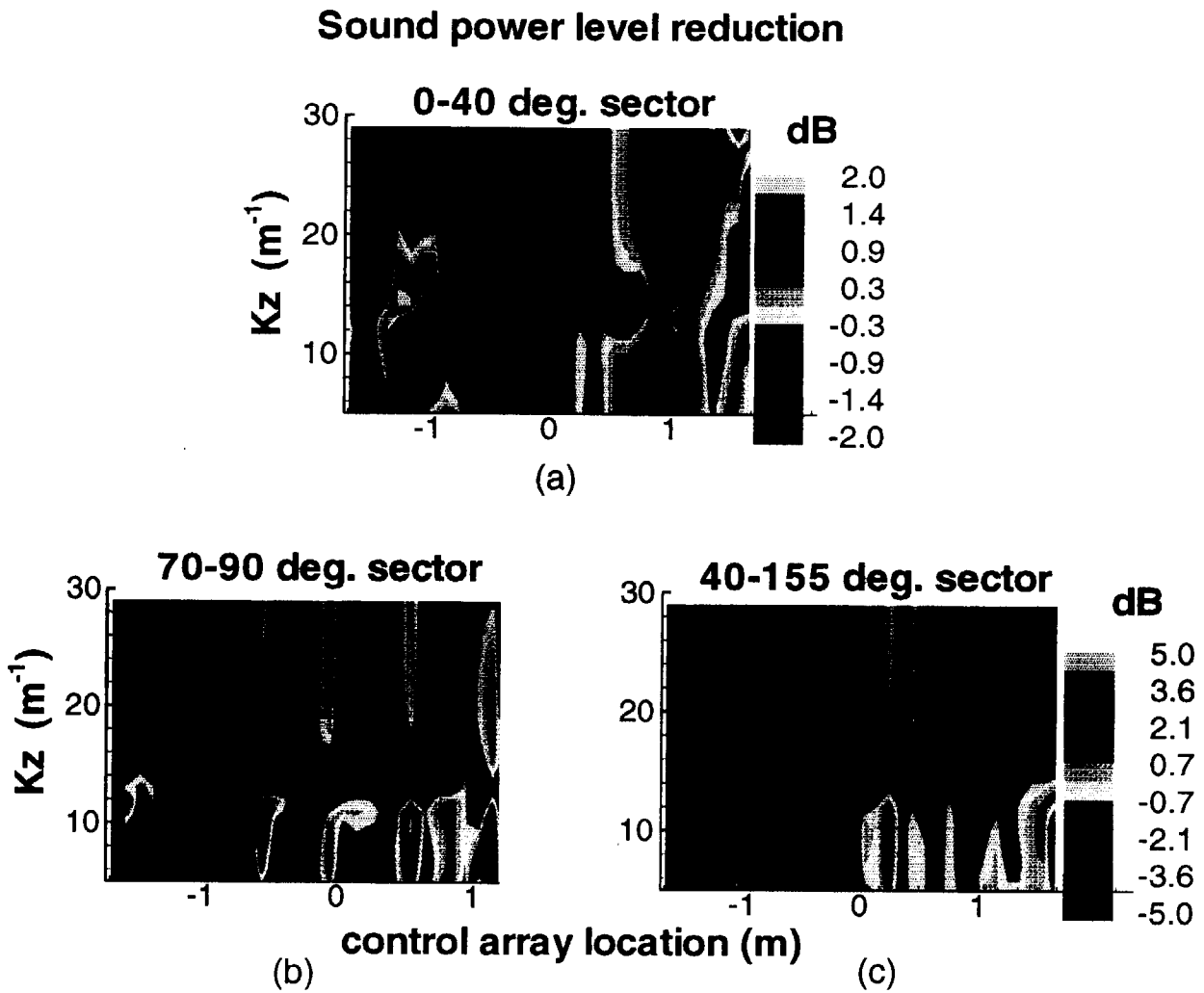

Figure 2.18: Sound power level reduction for the (a) 0-40 deg. sector, (b) 70-90 deg. sector, (c) target sector using the wavenumber technique. Pure ANC, 6 inlet sensors, resolution= 12.56 m^{-1}.

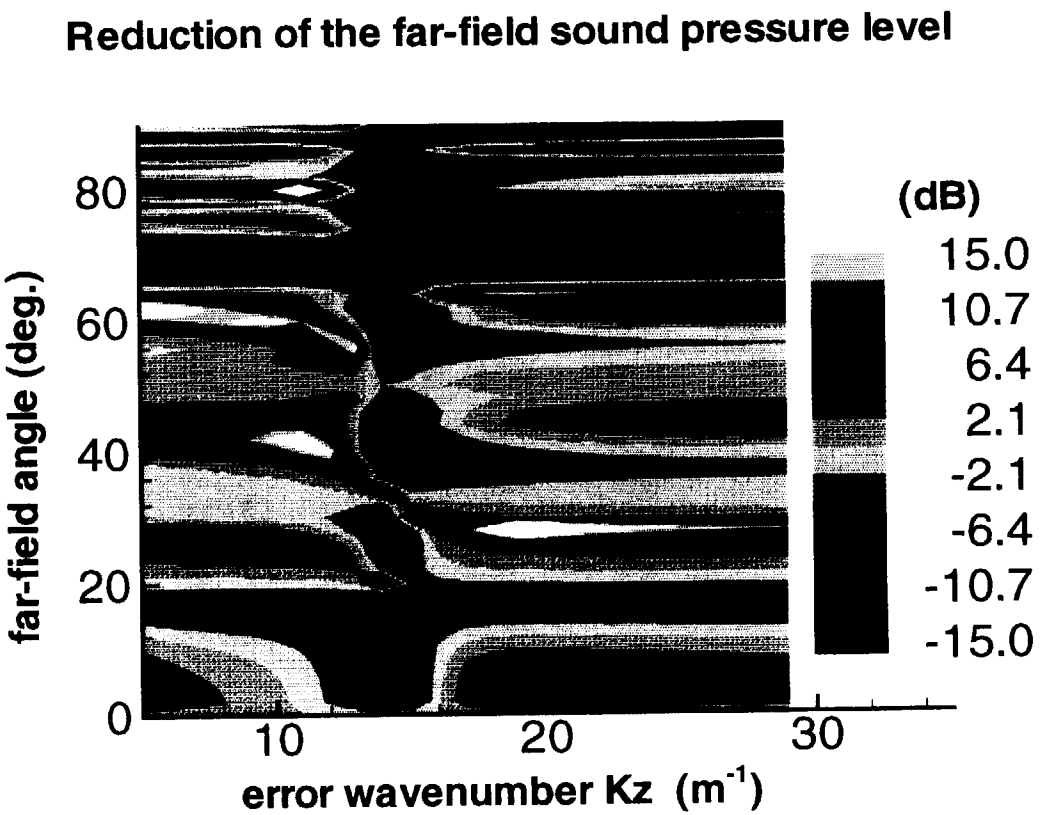

Figure 2.19: Far field sound pressure level reduction as a function of the error wavenumber. Pure ANC, Zc=0.25m.

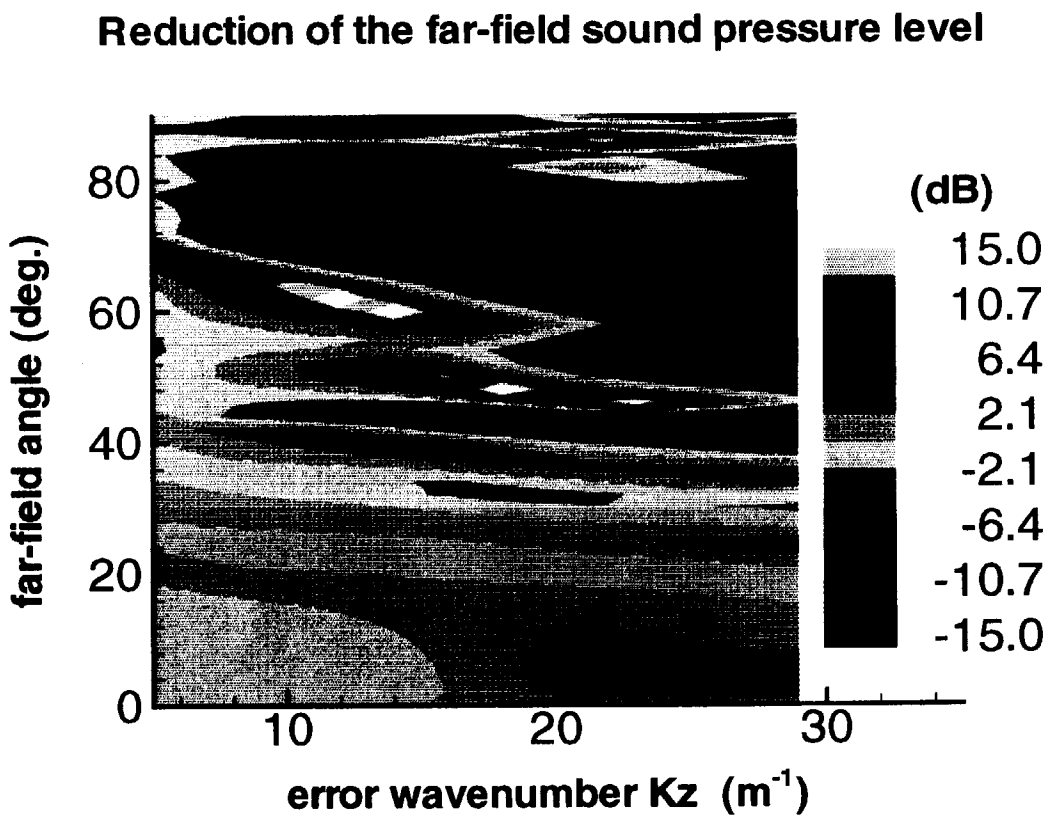

Figure 2.20: Far field sound pressure level reduction as a function of the error wavenumber. Hybrid system, Zc=-1.55 m.

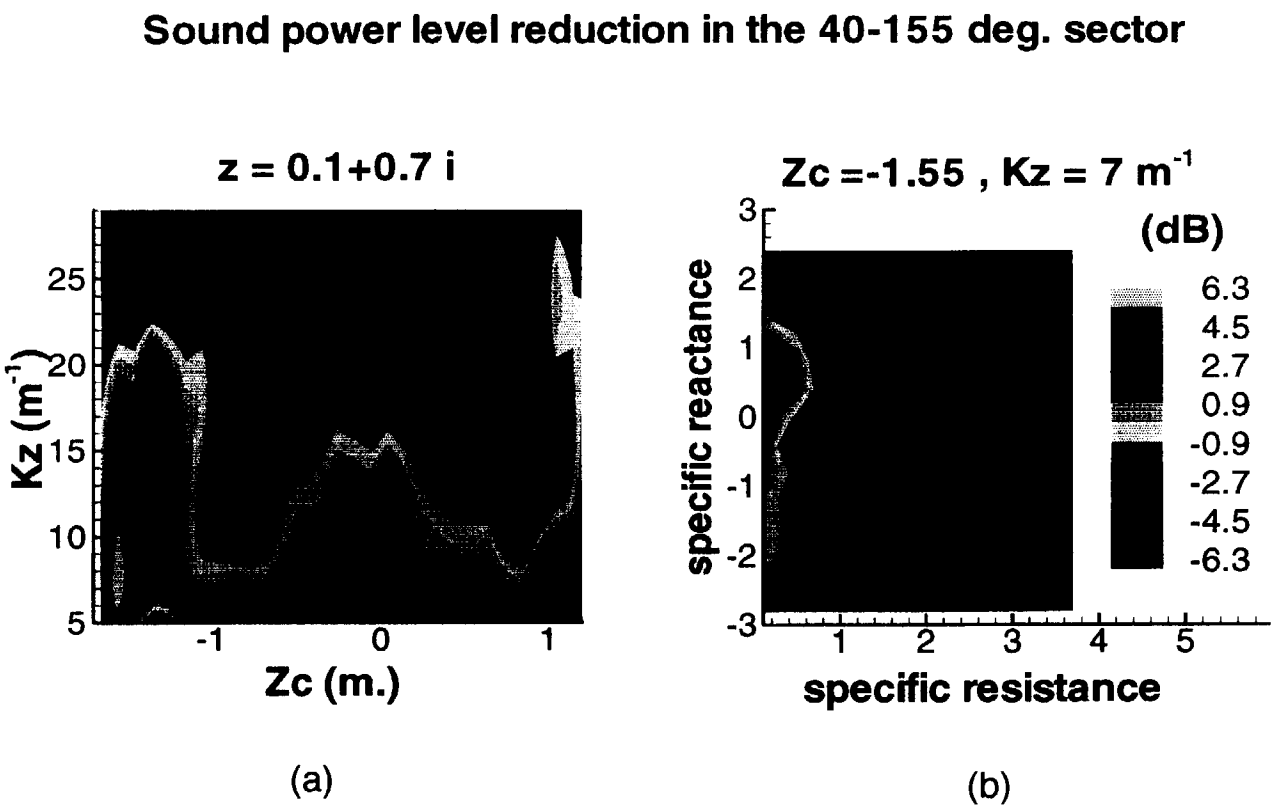

Figure 2.21: Reduction in sound power level for the target sector with (a) optimum liner, (b) optimum control array location and error wavenumber. Wavenumber technique; hybrid control; inlet sensors.

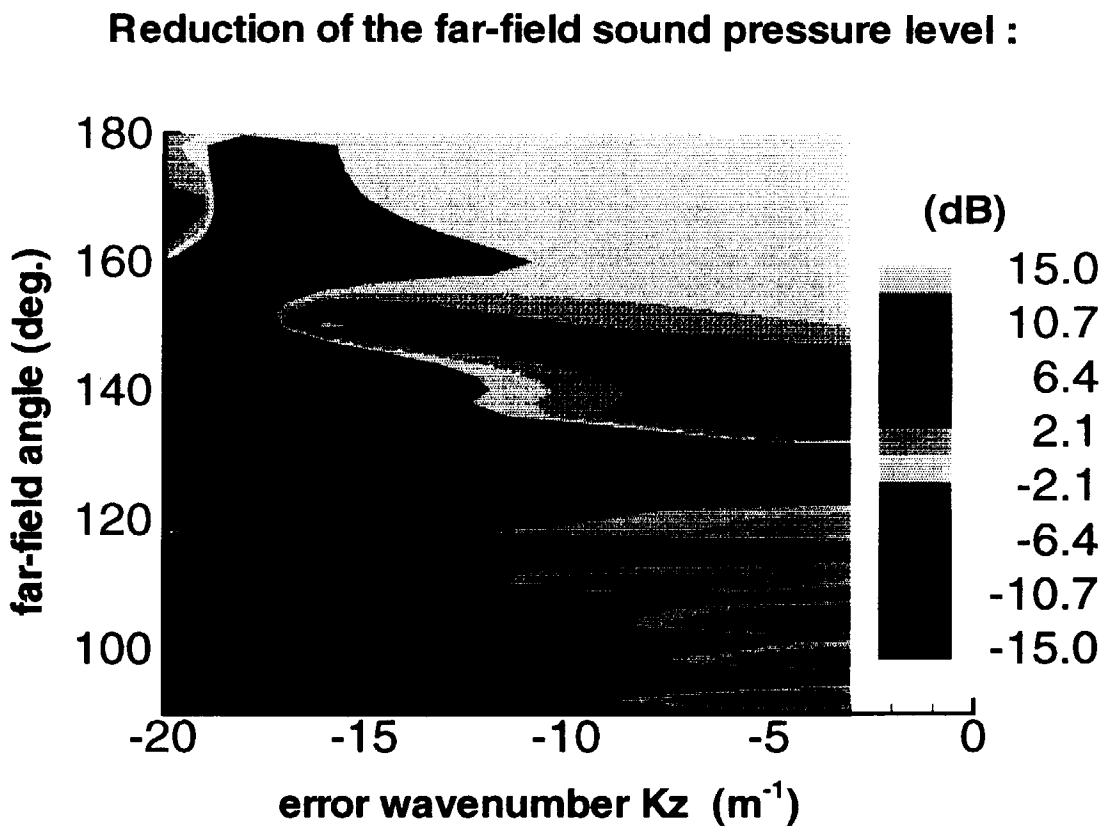

Figure 2.22: Far field sound pressure level reduction as a function of the error wavenumber. Hybrid control, outlet sensors, Zc=0.25m.

ΔSPWL(40-155)° in (dB) :		Fuselage sensors technique			wavenumber technique	
		inlet radiation		inlet + outlet radiation	⊕ve Kz	⊖ve Kz
Pure ANC		3 sensors	7 sensors			
1 control array		2.3	2.9	2.03	2.3	
2 control arrays		5.3	6.0	4.3		
Hybrid control						
1 control array		8.4		7.3	6.3	8.3
2 control arrays			10.2	9.6		
Pure passive	4.5					

Figure 2.23: Summary of the optimum levels of reduction that could be achieved for the target sector by the different control systems studied.

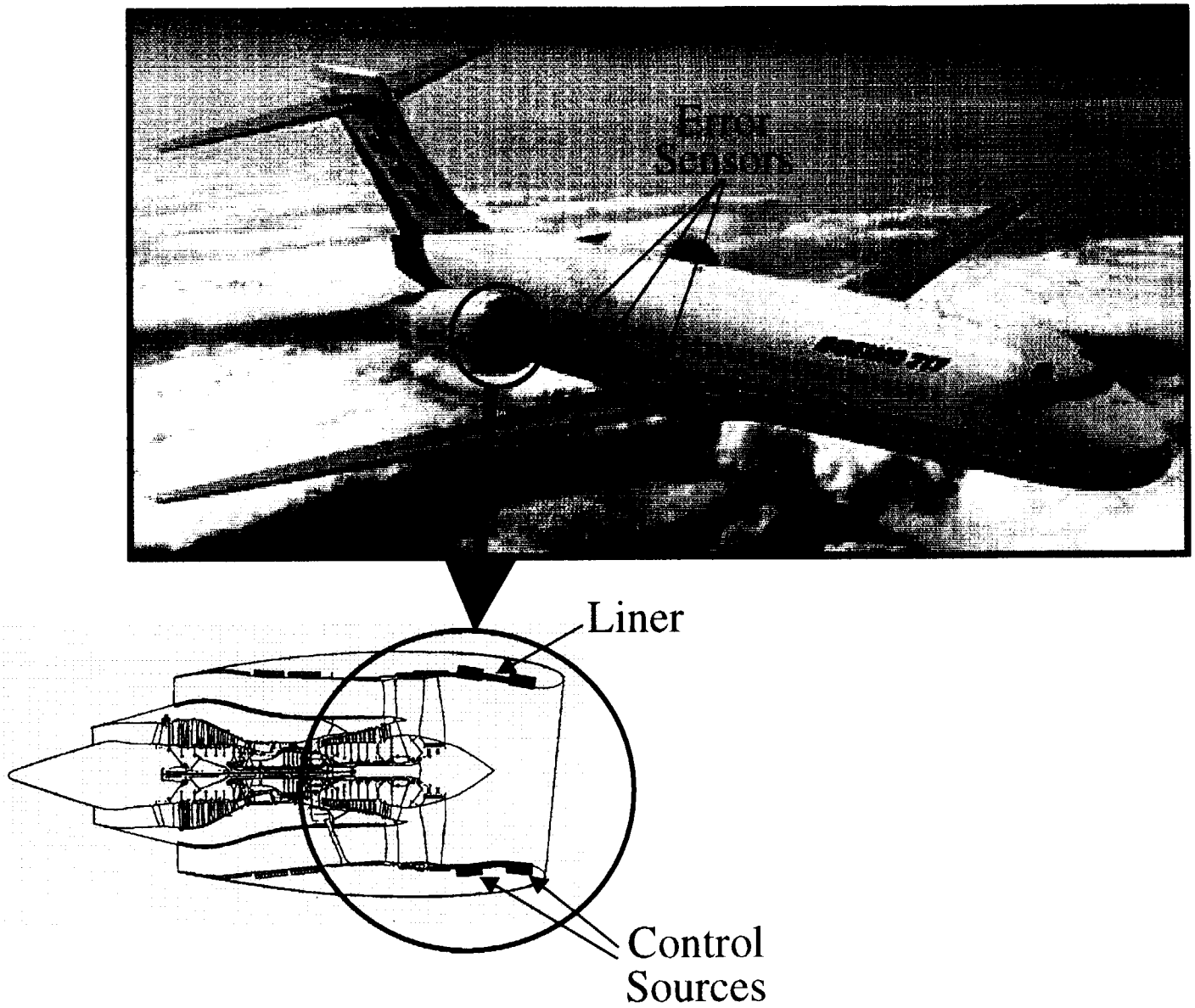

Figure 1.1: Depiction of the concept of ANC with fuselage-mounted error sensors on a Boeing 717.

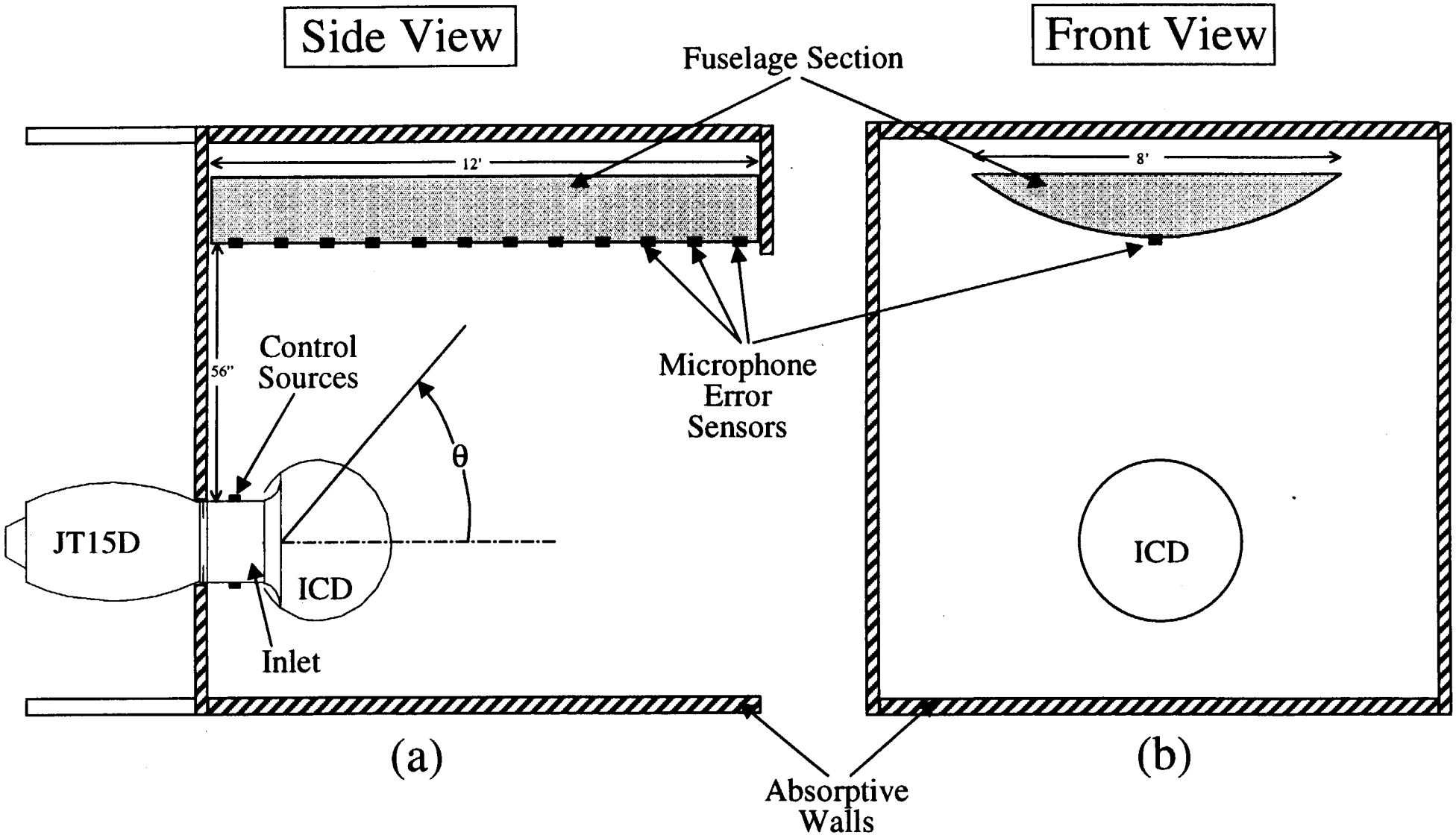

Figure 3.1: Schematic of the experimental JT15D test cell configuration, (a) side view, (b) front view.

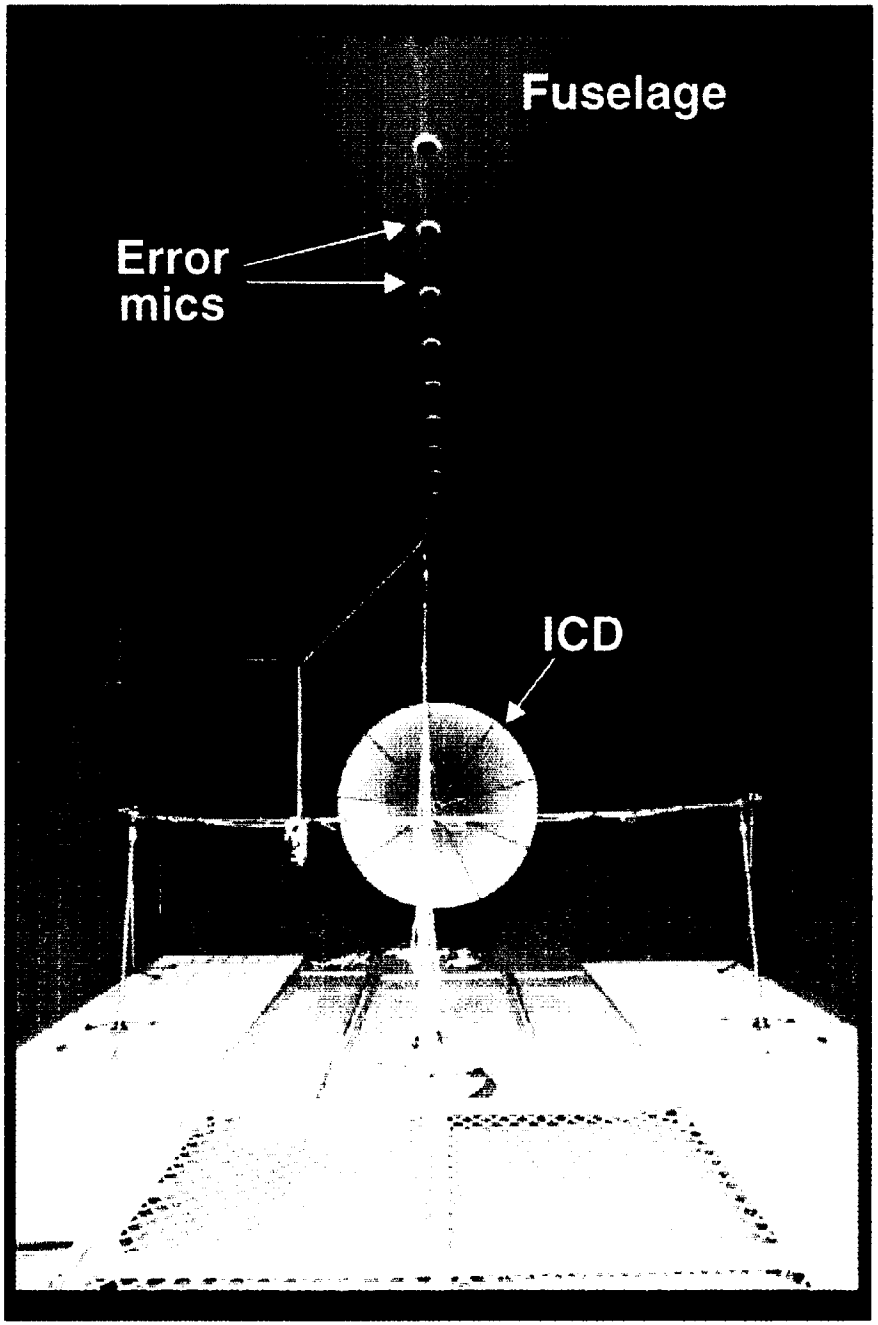

Figure 3.2: Front-on picture of the JT15D test cell configuration.

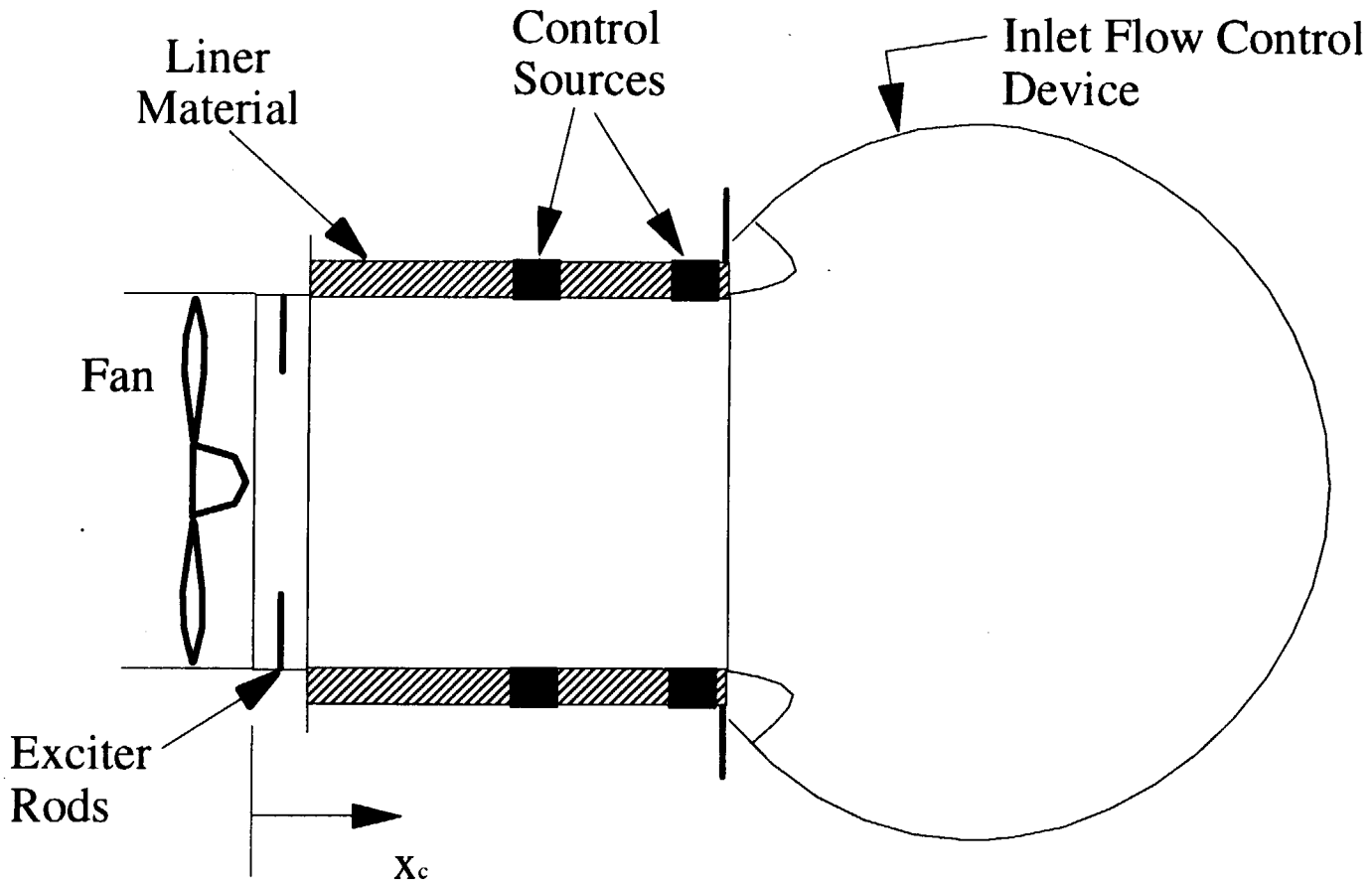

Figure 3.3: Schematic of the JT15D inlet configuration.

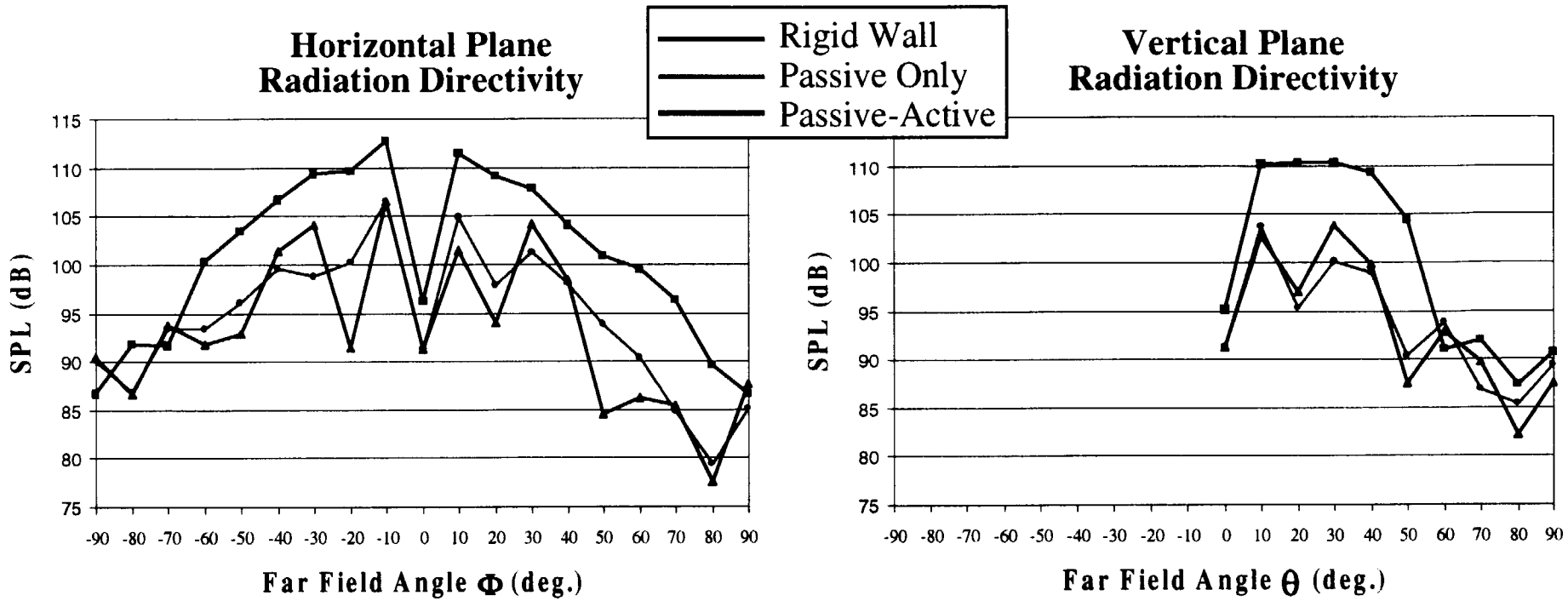

(a) (b)

Additional Power Reduction due to ANC (dB)

Sector	Passive-Active
Total	-0.8
50° to 70°	1.7
50° to 90°	1.6

(c)

Figure 3.4: ANC results at BPF tone with a 1C4E system, x_{e1} = 0.30 m, four error sensors on fuselage at θ=45°, θ=57°, θ=65°, θ=74°, BPF = 2328 Hz, (a) horizontal plane radiation directivity, (b) vertical plane radiation directivity, (c) table of additional power reduction achieved with ANC over sectors..

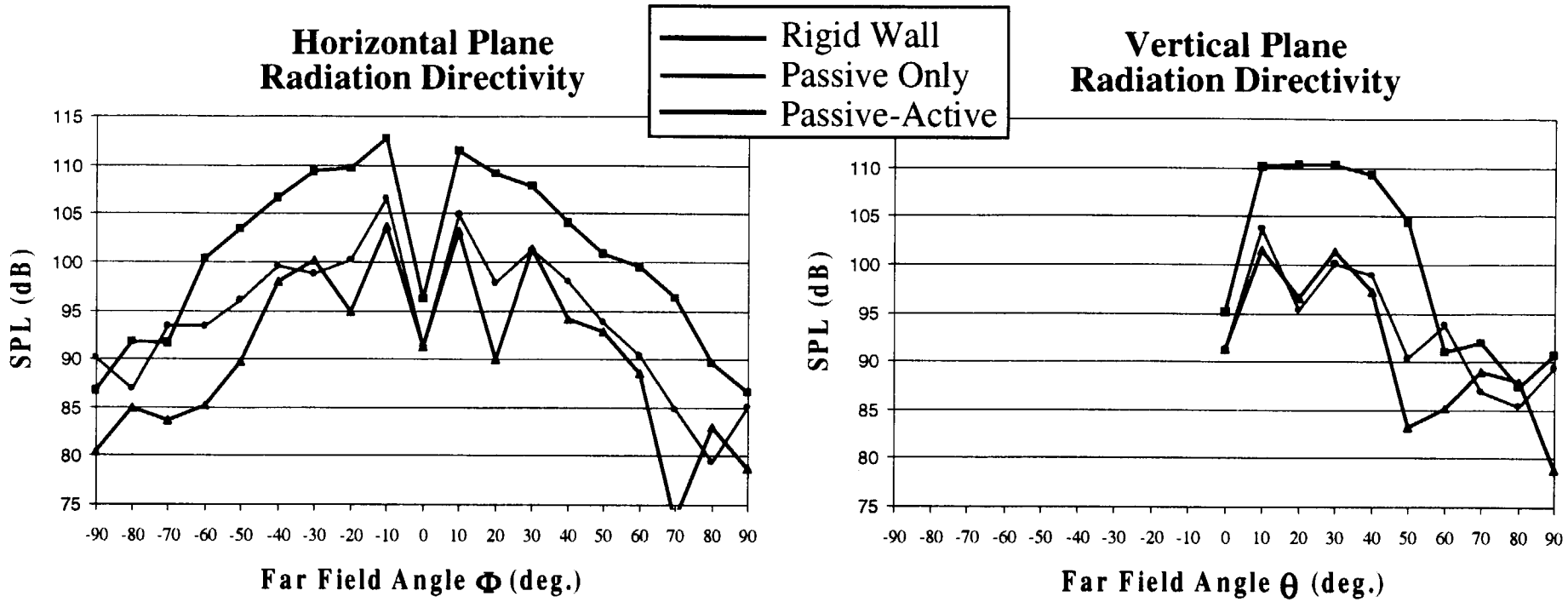

Additional Power Reduction due to ANC (dB)

Sector	Passive-Active
Total	1.8
50° to 70°	4.7
50° to 90°	4.3

(c)

Figure 3.5: ANC results at BPF tone with a 2C4E system, x_{c1}= 0.30 mand x_{c2}= 0.48 m, four error sensors on fuselage at θ=40°, θ=45°, θ=50°, θ=57°, BPF = 2328 Hz, (a) horizontal plane radiation directivity, (b) vertical plane radiation directivity, (c) table of additional power reduction achieved with ANC over sectors..

o28e1

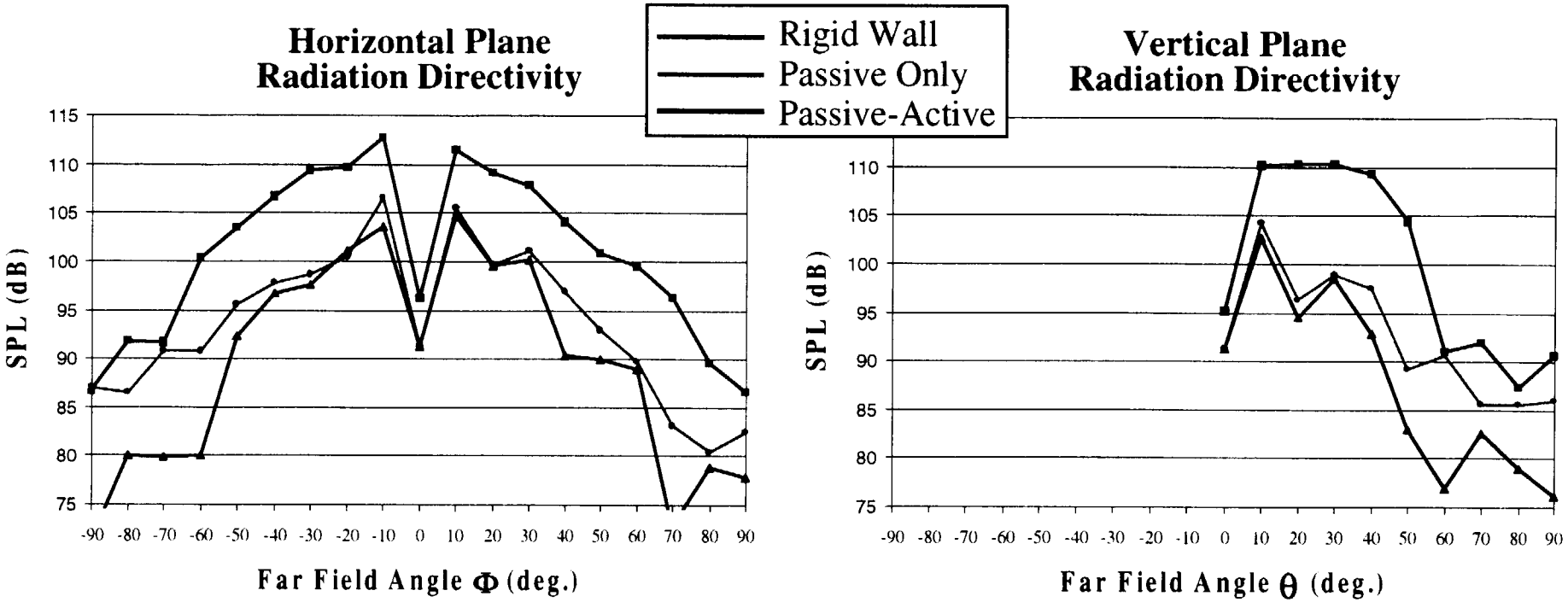

Additional Power Reduction due to ANC (dB)

Sector	Passive-Active
Total	1.8
50° to 70°	4.5
50° to 90°	4.8

(c)

Figure 3.6: ANC results at BPF tone with a 2C2E system, x_{c1}= 0.30 mand x_{c2}= 0.48 m, two error sensors on fuselage at θ=57°, θ=65°, BPF = 2324 Hz, (a) horizontal plane radiation directivity, (b) vertical plane radiation directivity, (c) table of additional power reduction achieved with ANC over sectors..

o30e3

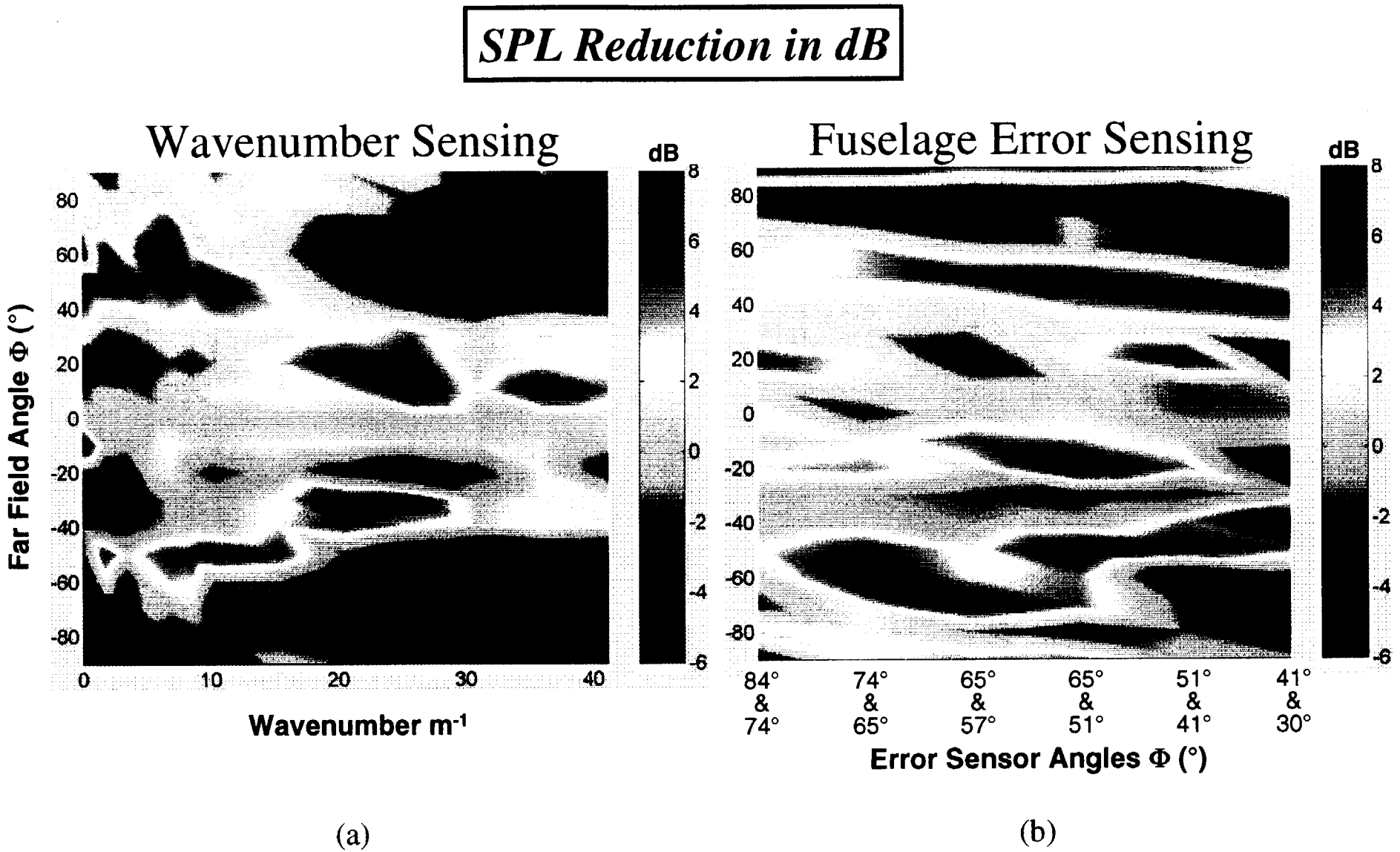

Figure 3.7: Comparison of ANC with fuselage error sensors to ANC with wavenumber sensing, (a) SPL reduction vs. far field angle and wavenumber minimized, (b) SPL reduction vs. far field angle and fuselage mounted error sensor locations.

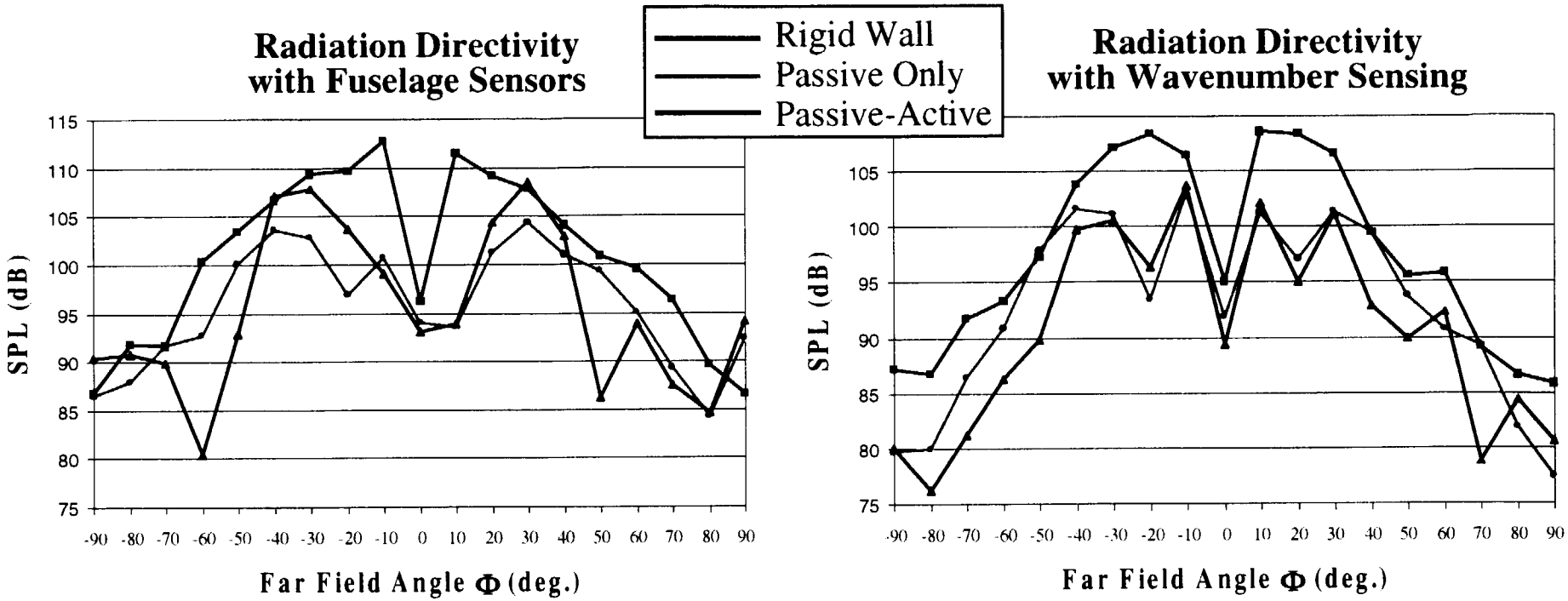

(a) (b)

Additional Power Reduction due to ANC (dB)

Sector	Fuselage Sensing 1C1E	Wavenum. Sensing 1C1E
Total	-2.0	1.0
50° to 70°	6.7	4.9
50° to 90°	5.0	4.7

(c)

Figure 3.8: Comparison of ANC with FES to WNS, (a) horizontal plane radiation directivity 1C1E FES system, x_{c1}= 0.30 m, one error sensor on fuselage at θ=50°, BPF = 2320 Hz, (b) horizontal plane radiation directivity 1C1E WNS system, x_{c1}= 0.30 m, one wavenumber sensor observing k_x = 5.2 m^{-1}, BPF = 2320 Hz, (c) table of additional power reduction achieved with each method over sectors.

813e9
o22e14

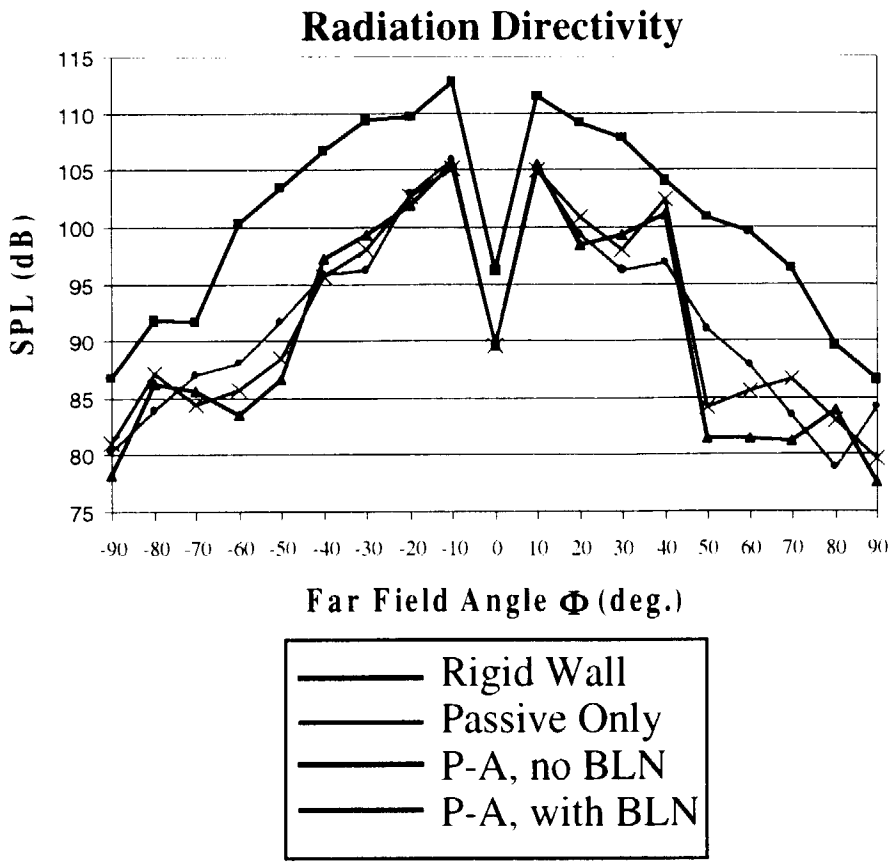

(a)

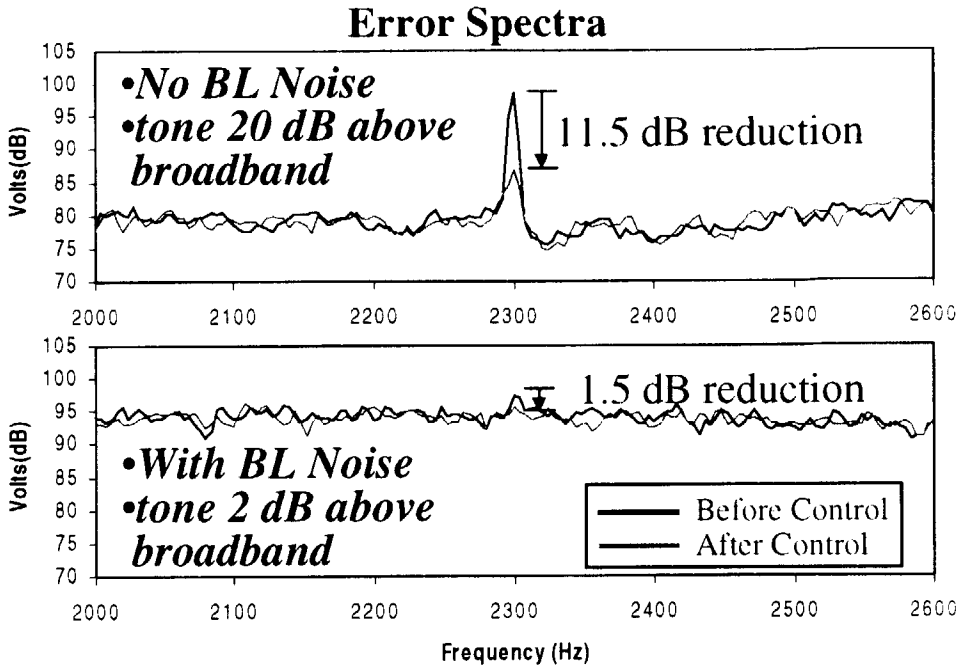

(b)

Additional Power Reduction due to ANC (dB)

Sector	Passive-Active No BLN	Passive-Active With BLN
Total	-0.5	-1.1
50° to 70°	2.9	1.6
50° to 90°	2.4	1.3

(c)

Figure 3.9: Results of ANC with FES and addition of simulated boundary layer noise (a) horizontal plane radiation directivities 1C1E FES system, x_{c1}= 0.30 m, one error sensor on fuselage at θ=57°, BPF = 2300 Hz, (b) corresponding error sensor spectra before and after control, (c) table of additional power reduction achieved with each method over sectors.

n6e3
n6e4